J. Fluid Mech. (1997), *vol.* 347, *pp.* 71–103. Printed in the United Kingdom

Generalized critical-layer analysis of fully coupled resonant-triad interactions in boundary layers

By SANG SOO LEE

NYMA, Inc., NASA Lewis Research Center Group, MS 5-9,
Cleveland, OH 44135, USA

(Received 25 May 1994 and in revised form 2 June 1997)

The critical-layer analysis of the nonlinear resonant-triad interaction by Goldstein & Lee (1992) is extended to include viscous effects. A generalized scaling which is valid both for the quasi-equilibrium and non-equilibrium critical-layer analyses in zero- or non-zero-pressure-gradient boundary layers is obtained. A system of partial differential equations which governs the fully coupled non-equilibrium critical-layer dynamics is obtained and it is solved by using a numerical method. Amplitude equations and their viscous limits are also presented. The parametric-resonance growth rate of the non-equilibrium critical-layer solution with finite viscosity is larger than that of the viscous-limit quasi-equilibrium solution. The viscosity delays both the onset of the fully coupled interaction and the ultimate downstream location of the singularity. The difference between the non-equilibrium critical-layer solution and the corresponding quasi-equilibrium critical-layer solution becomes smaller, at least in the parametric resonance region, as the viscosity parameter becomes large. However, the non-equilibrium solution with finite viscosity always ends in a singularity at a finite downstream position unlike the viscous-limit solution.

1. Introduction

Boundary-layer transition experiments usually involve spatially growing instability waves whose initial two-dimensional and linear behaviour can persist over long streamwise distance when the excitation levels are sufficiently small. But three-dimensional effects eventually come into play, as evidenced by the appearance of Λ-shaped structures in flow-visualization experiments. These structures can either be aligned or staggered in alternating rows. It is now believed that the staggered arrangement is the result of a resonant-triad interaction between a pair of oblique subharmonic modes and the basic fundamental two-dimensional mode. This interaction was analysed for the case of viscous-dominated Tollmien–Schlichting-type instabilities by Raetz (1959) and was studied in considerably more detail by Craik (1971), who proposed that the unstaggered (or aligned) arrangement could also result from a resonant-triad interaction, which would then involve a pair of oblique fundamental harmonic modes interacting with the small two-dimensional first harmonic mode.

Since transition in technological devices usually occurs in a region of adverse pressure gradient, Goldstein & Lee (1992) (hereafter referred to as G&L) analysed the resonant-triad interaction in a boundary-layer flow with a relatively weak adverse

pressure gradient. The wavelength in their analyses is therefore large, O(adverse pressure gradient)$^{-1/2}$, and their results show that the oblique mode does not affect the plane wave until its amplitude exceeds that of the plane wave by a factor of the wavenumber cubed. Wundrow, Hultgren & Goldstein (1994) also analysed the adverse-pressure-gradient boundary layer, but with smaller initial oblique mode amplitude than in G&L. The Blasius boundary-layer flow was studied by Mankbadi, Wu & Lee (1993) and the boundary-layer flow with $O(1)$ favourable pressure gradient was studied by Wu (1993) in the quasi-equilibrium limit. Khokhlov (1993) studied the parametric-resonance stage of the resonant-triad interaction. Wu, Lee & Cowley (1993) and Wu (1995) considered the effects of finite viscosity in non-equilibrium critical layers. They obtained the kernel functions and amplitude equations for the two-oblique-mode and full resonant-triad interactions respectively. The integro-differential equations for the instability wave amplitudes are of the same form as in the inviscid case, but with viscous kernel functions. Asymptotic analyses of instability waves in high-Reynolds-number flows, including critical-layer analyses, are reviewed by Cowley & Wu (1994).

The type of critical layer that governs the interactions is determined both by the type of problem and by the initial amplitudes of the instability waves. The growth and mean convection (and also viscous) effects can enter the critical-layer dynamics at the same order, which we refer to as the non-equilibrium critical-layer dynamics, as in G&L. However, when the viscous effect becomes large, the mean convection effect balances with the viscous effect inside the critical layer, which we refer to as a (viscous) quasi-equilibrium (or viscous limit) critical layer, as in Mankbadi *et al.* (1993) and Wu (1993).

Since most excitation devices tend to be two-dimensional, the initial oblique-mode amplitudes should be much smaller than the initial plane-wave amplitude. The initial nonlinear interaction will then be a secondary instability that leaves the plane-wave growth rate unchanged while greatly enhancing the growth rate of the oblique modes. This might be termed the 'parametric resonance' stage. The nonlinear critical-layer studies mentioned above indicate that the initial nonlinear interaction produces no critical-layer velocity jump at the fundamental frequency, which means that the two-dimensional mode continues to grow at its initial linear growth rate, even when the oblique modes become very large relative to the plane wave. This, in turn, allows these latter modes to exhibit faster-than-exponential growth even when they are much larger than the more slowly growing two-dimensional mode.

The non-equilibrium critical-layer analysis of G&L shows that the oblique modes eventually react back on the two-dimensional mode, which might be termed the 'fully coupled' stage. The corresponding 'back-reaction' term turns out to be quartic in the oblique-mode amplitudes. The oblique modes also interact nonlinearly within their common critical layer to produce a 'self-interaction' term which has a dramatic effect on the subsequent instability-wave development. This term causes the instability growth to increase beyond the faster-than-exponential growth of the parametric-resonance stage and ultimately leads to a singularity at a finite downstream position. In the non-equilibrium analyses of G&L, Wu (1992) and Wundrow *et al.* (1994), the nonlinear interactions are completely confined to the critical layers.

As shown in Wundrow *et al.* (1994), the plane wave can become strongly nonlinear within its own critical layer (as in Goldstein, Durbin & Leib 1987) before it is affected by the oblique mode when the initial amplitude of the oblique mode, which is the only difference in starting conditions between this and G&L's analyses, is sufficiently small. The growth of the oblique mode becomes dominated by the parametric-resonance

interaction and occurs on a much shorter streamwise scale than that of the plane wave. The oblique-mode amplitude continues to increase during the parametric-resonance stage and eventually becomes large enough to react back on the two-dimensional mode, which causes oblique and plane waves to evolve on the same shorter streamwise scale. This fully coupled stage is governed by the same amplitude equation as in G&L – but with the linear growth terms omitted.

The quasi-equilibrium analyses of Mankbadi *et al.* (1993) and Wu (1993) involve viscous critical layers with the dominant nonlinear interactions taking place in an intermediate diffusion layer that surrounds the critical layer and lies inside the inviscid wall layer. There is no back-reaction effect on the plane wave which therefore continues to grow linearly.

Goldstein (1994, 1995) shows that the initial parametric resonance growth of quasi-equilibrium type in a Blasius boundary layer will be followed by the non-equilibrium-type interaction before the self-interaction effect becomes important when the initial oblique-mode amplitude is sufficiently (or exponentially) small at the start of parametric resonance. This occurs because the growth rate continuously increases during the parametric-resonance stage which causes the critical layer to become of the non-equilibrium type by the time self-interaction effects come into play. The final critical-layer stage is then of the fully coupled non-equilibrium type considered by G&L rather than the quasi-equilibrium type of Mankbadi *et al.* (1993).

Wu, Leib & Goldstein (1997) show that a pair of oblique Tollmien–Schlichting waves, which are initially linear, can evolve through several nonlinear stages when the initial plane wave amplitude is smaller than that in Mankbadi *et al.* (1993). However, the critical layer eventually becomes of the non-equilibrium type even though the critical layers in previous stages are of the quasi-equilibrium type.

These recent studies indicate that the final nonlinear critical-layer stage is governed by non-equilibrium dynamics rather than being dominated by viscous (i.e. quasi-equilibrium) effects. The present study extends the resonant-triad critical-layer analysis of G&L to include viscous effects. A generalized scaling which is valid for the fully coupled critical-layer analyses of resonant-triad of long-wavelength small-growth-rate instability waves in zero- or non-zero-pressure-gradient boundary layers is obtained. A system of partial differential critical-layer equations governing the non-equilibrium critical-layer dynamics is derived and solved numerically.

The overall plan of the paper is as follows. The problem is formulated in §2 and the generalized scaling is presented in §3. A generalized non-equilibrium critical-layer analysis is given in §4 to §6. The solutions in the main boundary layer are given in §4. In §5 we show that the linear Tollmien solution for the inviscid wall layer can be matched onto the solution of §4. The critical-layer equations and the jump conditions are obtained in §6 and the upstream matching is discussed. The numerical method is described in §7. Analytical solutions of the critical-layer equations and the resulting amplitude equations (including their viscous limit) are summarized in §8. The Blasius boundary layer flow is considered in §9 and matching with the initial linear critical layer is discussed. The numerical results are given in §10.

2. Formulation

We suppose that the mean boundary-layer flow is two-dimensional and that the local Reynolds number $R_{\Delta}(= U_{\infty}\Delta/\nu)$, based on the local free-stream velocity U_{∞} and the local boundary-layer thickness Δ, is sufficiently large that the unsteady flow is nearly inviscid in the main part of the boundary layer and is nearly unaffected

by boundary-layer growth over the region in which nonlinear interaction takes place. The mean flow velocity U and the total flow velocity $\boldsymbol{u} = \{u, v, w\}$ are normalized by U_∞, the streamwise, transverse, and spanwise coordinates x, y, and z, respectively, are normalized by Δ, the pressure p is normalized by ρU_∞^2, and the time t is normalized by Δ/U_∞. The base mean flow is nearly parallel and develops slowly on the long viscous scale,

$$x_3 = x/R_\Delta. \tag{2.1}$$

The upstream flow can start as a resonant triad of spatially growing linear instability waves as in G&L, Mankbadi *et al.* (1993) and Wu (1993), or as a resonant triad of linear and nonlinear instability waves (which are solutions of the preceding linear or nonlinear stages) as in Wundrow *et al.* (1994) and Goldstein (1994). The resonant triad is composed of a single two-dimensional mode of frequency ω and wavenumber α and a pair of subharmonic oblique modes of frequency $\omega/2$, streamwise wavenumber nearly equal to $\alpha/2$ and spanwise wavenumbers $\pm\beta$.

The normalized complex wavenumber α is small and its imaginary part is much smaller than its real part. It follows that each of the three modes must have a critical layer at nearly the same transverse position, say y_c, where the mean flow velocity U is equal to the real part of their nearly common phase velocity.

3. Generalized scaling

The scaling in G&L was chosen so that the wavenumber scale σ corresponded to the most rapidly growing linear instability mode in an adverse-pressure-gradient boundary layer. We can generalize the scaling by not imposing that condition *a priori*. If we introduce parameters σ, σ^r and σ^m for the small wavenumber (long wavelength), the ratio of the small growth rate to the wavenumber and the non-equilibrium effect, respectively, we can obtain a generalized scaling which is valid both for the non-equilibrium and quasi-equilibrium critical layers. The mean convection effect balances with the growth (and viscous, for the finite viscous case) effects (see (6.4) and (6.25)) in the non-equilibrium critical layer (G&L), and with the viscous effect in the quasi-equilibrium (or viscous limit) critical layer (Mankbadi *et al.* 1993; Wu 1993).

The non-equilibrium parameter m will be

$$0 \leqslant m \leqslant r, \tag{3.1}$$

where m is equal to zero when the critical layer is of the viscous-dominated (i.e. quasi-equilibrium) type as in Mankbadi *et al.* (1993) and Wu (1993) and is equal to r for the non-equilibrium critical layer considered in G&L. The generalized scaling can be written as

$$\alpha = \sigma[\bar{\alpha} + O(\sigma^r)], \quad c_0 = \sigma[\bar{c} + O(\sigma^r)], \quad \beta = \sigma\bar{\beta}, \quad y_c = \sigma Y_c, \tag{3.2}$$

$$\mu = \sigma^{r-1}\bar{\mu}\left(= R_\Delta \frac{\mathrm{d}P}{\mathrm{d}x}\right), \tag{3.3}$$

and

$$x_1 = \sigma^{r+1}x, \tag{3.4}$$

where σ characterizes the small wavenumber, c_0 is the phase velocity of the two-dimensional mode, $\bar{\alpha}$, $\bar{c}$, $\bar{\beta}$ and Y_c are order-one real constants (which depend on σ) and μ is the normalized mean pressure gradient. When $\bar{\mu}$ is an order-one real positive constant, $\sigma^{r-1}\bar{\mu} \ll 1$ characterizes a small adverse pressure gradient as in the G&L

analysis. However, we now allow $\bar{\mu}$ to be non-positive in order to extend the scaling to the important Blasius and favourable-pressure-gradient boundary layers.

As shown in G&L, Mankbadi *et al.* (1993), Wu (1993), and others, viscous effects will enter the critical-layer momentum equation while making only relatively insignificant modifications to the external flow when the viscous parameter (Benney & Bergeron 1969; Haberman 1972)

$$\lambda \equiv 1/(\sigma^{2r+m+4} R_{\Delta}) \tag{3.5}$$

is order one.

When $\bar{\mu}$ is $O(1)$ or $r = 3$ as in G&L, Mankbadi *et al.* (1993) and Wu (1993), the linear-growth and parametric-resonance effects enter the oblique-mode critical-layer dynamics at the same order if the amplitude scaling of the two-dimensional instability wave ϵ_{2d} is given by

$$\epsilon_{2d} = \sigma^{3r+m+1}. \tag{3.6}$$

The non-zero velocity jump across the critical layer for the non-equilibrium critical-layer case (G&L) or across the diffusion layer for the quasi-equilibrium critical-layer case (Mankbadi *et al.* 1993; Wu 1993) produced by the self-interaction between the oblique modes will balance the corresponding growth rate term when

$$\delta_{3d} = \sigma^{(7r+2m)/3+1}, \tag{3.7}$$

where δ_{3d} is a measure of the (common) amplitude of the oblique modes. The nonlinear effects in the critical layer produce a mean flow correction term which is periodic in the spanwise direction with the spanwise wavenumber equal to 2β, as was first shown in Goldstein & Choi (1989). This term is large in the sense that its magnitude

$$\delta_{02} = \delta_{3d}/\sigma^{(r-m)/3} = \sigma^{2r+m+1}, \tag{3.8}$$

is larger than or equal to the magnitude of the oblique waves.

The nonlinear interactions between instability waves occur within the thin critical layer whose transverse coordinate scales like

$$\bar{\eta} = \frac{y - y_c}{\sigma^{(2r+m)/3+1}}. \tag{3.9}$$

The quasi-equilibrium analyses of Mankbadi *et al.* (1993) and Wu (1993) show that the nonlinearly generated mean flow interacts with the oblique modes in a diffusion layer to produce the self-interaction term in the amplitude equation. The thickness of this diffusion layer, which surrounds the critical layer, is given by

$$\hat{\eta} = \frac{y - y_c}{\sigma^{(r+m)/2+1}}. \tag{3.10}$$

The viscous Stokes layer close to the wall contributes to the linear growth rate when the viscous effects are large, as in the Blasius and favourable-pressure-gradient boundary layers (Mankbadi *et al.* 1993; Wu 1993). The appropriately scaled transverse coordinate for this layer is

$$\hat{y} = \frac{y}{\sigma^{r+m/2+1}}. \tag{3.11}$$

The generalized scaling (3.2)–(3.11) is valid for the fully coupled critical-layer analyses of resonant triads in zero- or adverse/favourable-pressure-gradient boundary layers (with long-wavelength small-growth-rate instability waves). The diffusion-layer thickness in (3.10) becomes the same as that of the critical layer in (3.9) when $m = r$ or

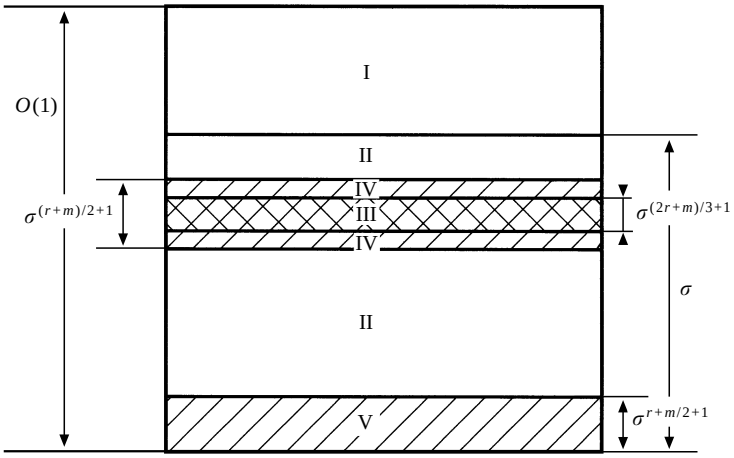

FIGURE 1. Multi-layer structure in boundary layers. I, main boundary layer; II, inviscid Tollmien wall layer; III, critical layer; IV, diffusion layer; V, viscous Stokes layer.

equivalently when the critical layer is of non-equilibrium type. A schematic diagram of the multi-layer structure is given in figure 1.

We can recover the scalings of previous studies described above by appropriately choosing the parameters in the present scaling. As indicated in table 1, the adverse-pressure-gradient boundary layer in G&L corresponds to the case when $r = m = 3$, the Blasius boundary layer in Mankbadi *et al.* (1993) corresponds to the case when $r = 3$ and $m = \bar{\mu} = 0$ and the favourable-pressure-gradient boundary layer considered by Wu (1993) corresponds to the case where $r = 1$ and $m = 0$. We can also recover the scalings for the later fully coupled stage of the adverse-pressure-gradient boundary layer with initially small subharmonic amplitude in Wundrow *et al.* (1994) by putting $r = m = 3/2$ and $\bar{\mu} = \lambda = 0$ and the later fully coupled stage of the Blasius boundary layer considered in Goldstein (1994) by putting $r = m = 2$ and $\bar{\mu} = 0$.

One of the new interesting scalings can be obtained by taking $r = 3$ and $m = 0$, which is a version of order-one $\bar{\mu}$ of the quasi-equilibrium critical-layer scaling of Mankbadi *et al.* (1993), as shown in table 1. This scaling applies to the boundary layer with small non-zero pressure gradient, i.e. the adverse-pressure-gradient boundary layer where the viscous effect is larger than in G&L or the boundary layer with smaller favourable pressure gradient than in Wu (1993). We will show in §8 that the governing amplitude equations are the same as those of Mankbadi *et al.* (1993) if their linear growth rates are modified to include the pressure-gradient effect (i.e. the first term on the right-hand side of (6.27)).

The scalings of the diffusion and viscous Stokes layers for the non-equilibrium critical-layer analyses in table 1 are given in parentheses because they correspond to higher-order terms in these problems. The scalings that would produce order-one pressure gradient and viscous effects are enclosed in square brackets. However, the actual values of these quantities considered in the indicated analyses are negligibly small. The linear growth rates of the instability waves become negligibly small when $\bar{\mu} \ll 1$ and $r < 3$, as will be shown in §6.

The scaling of the non-equilibrium critical-layer stage in Wu *et al.* (1997) is the same as in Goldstein (1994). However, the plane wave amplitude is negligibly small in the former. Both analyses consider the later stages of the evolution of the Tollmien–Schlichting waves in a Blasius boundary layer. Goldstein's (1994) analysis starts with

	r	m	$\alpha/\bar{\alpha}$	$\mu/\bar{\mu}$	$(\lambda R_\Delta)^{-1}$	x_1/x	ϵ_{2d}	δ_{3d}	δ_{02}	$(y-y_c)/\bar{\eta}$	$(y-y_c)/\hat{\eta}$	$y/\hat{y}$
Generalized scaling (present paper)	r	m	σ	σ^{r-1}	σ^{2r+m+4}	σ^{r+1}	σ^{3r+m+1}	$\sigma^{(7r+2m)/3+1}$	σ^{2r+m+1}	$\sigma^{(2r+m)/3+1}$	$\sigma^{(r+m)/2+1}$	$\sigma^{r+m/2+1}$
Goldstein & Lee (1992)	3	3	σ	σ^2	σ^{13}	σ^4	σ^{13}	σ^{10}	σ^{10}	σ^4	(σ^4)	$(\sigma^{11/2})$
Mankbadi *et al.* (1993)	3	0	σ	$[\sigma^2]$	σ^{10}	σ^4	σ^{10}	σ^8	σ^7	σ^3	$\sigma^{5/2}$	σ^4
Wu (1993)	1	0	σ	1	σ^6	σ^2	σ^4	$\sigma^{10/3}$	σ^3	$\sigma^{5/3}$	$\sigma^{3/2}$	σ^2
Wundrow *et al.* (1994)	3/2	3/2	σ	$[\sigma^{1/2}]$	$[\sigma^{17/2}]$	$\sigma^{5/2}$	σ^7	$\sigma^{11/2}$	$\sigma^{11/2}$	$\sigma^{5/2}$	$(\sigma^{5/2})$	$(\sigma^{13/4})$
Goldstein (1994)	2	2	σ	$[\sigma]$	σ^{10}	σ^3	σ^9	σ^7	σ^7	σ^3	(σ^3)	(σ^4)

TABLE 1. Generalized scaling of the resonant-triad interactions of long-wavelength small-growth-rate instability waves in boundary layers. $\bar{\alpha}$, $\bar{\mu}$ and λ are $O(1)$ constants. $\bar{\eta}$, $\hat{\eta}$ and $\hat{y}$ represent the scaled transverse coordinates in the critical, diffusion and viscous Stokes layers. The scalings in parentheses are not required for the leading-order analysis. For the scalings in square brackets, actual $\bar{\mu}$ and λ were negligibly small in the original analyses.

a linear resonant triad as in Mankbadi *et al.* (1993) but with sufficiently small initial amplitude of the oblique modes. The initial stage of Wu *et al.* (1997) only involves a pair of linear oblique modes, which coincides with the case where the initial plane wave amplitude is negligibly small in the Mankbadi *et al.* (1993) analysis. The instability waves in Wu *et al.* (1997) therefore follow a different route to the non-equilibrium stage than the one in Goldstein (1994). However, the oblique-mode amplitudes are ultimately governed by the same non-equilibrium scaling and amplitude equations in both cases.

Although it is possible to carry out the analysis for arbitrary m, for simplicity we will only give results for the non-equilibrium analysis where $m = r$. We will also assume that $1 \leqslant r \leqslant 3$ since table 1 indicates that this range of r covers most of the important types of boundary-layer flows. The analysis can easily be modified to include other values of r. The scalings in (3.5)–(3.9) now become

$$\lambda = 1/(\sigma^{3r+4} R_{\Delta}), \tag{3.12}$$

$$\epsilon_{2d} = \sigma^{4r+1}, \quad \delta_{3d} = \delta_{02} = \sigma^{3r+1}, \tag{3.13}$$

and

$$\bar{\eta} = \frac{y - y_c}{\sigma^{r+1}}. \tag{3.14}$$

Equations (3.12)–(3.14) along with (3.2)–(3.4) are the non-equilibrium version of the generalized scaling and these will be used in the following sections. We do not need to include the diffusion and viscous Stokes layers for this type of analysis. The thickness of the former becomes the same as that of the critical layer and the latter does not make a leading-order contribution to the growth rate.

4. Main boundary layer

In this and the following sections we derive dispersion relations connecting the phase speed and the wavenumbers of the instability waves. Since the analysis is now quite well documented we include only enough steps to guide the reader. We have attempted to use the same notation as G&L (except their U_0' being replaced by τ_0) and do not repeat some of the equations that are given in G&L.

The unsteady flow outside the critical layer is governed by linear dynamics to the required order of approximation, which means that the velocity field can be written as

$$u = U(y, x_3) + \epsilon_{2d} \mathrm{Re} A_0 \Phi_{0y} \mathrm{e}^{\mathrm{i}X} + \delta_{3d} \mathrm{Re} 2A\tilde{U}(y, x_1)\mathrm{e}^{\mathrm{i}X/2} \cos Z + \delta_{02} \mathrm{Re}\, \tilde{U}_{02}(y, x_1)\mathrm{e}^{2\mathrm{i}Z} + \ldots, \tag{4.1}$$

$$v = -\epsilon_{2d} \mathrm{Re}\mathrm{i}\alpha A_0(x_1)\Phi_0(y, x_1)\mathrm{e}^{\mathrm{i}X} - \delta_{3d} \mathrm{Re} 2\mathrm{i}\gamma A(x_1)\Phi(y, x_1)\mathrm{e}^{\mathrm{i}X/2} \cos Z + \ldots, \tag{4.2}$$

and

$$w = \delta_{3d} \mathrm{Re} 2\mathrm{i} A\tilde{W}(y, x_1)\mathrm{e}^{\mathrm{i}X/2} \sin Z + \ldots, \tag{4.3}$$

with

$$X \equiv \sigma\bar{\alpha}(x - \sigma\bar{c}t) \quad \text{and} \quad Z \equiv \sigma\bar{\beta}z, \tag{4.4}$$

where Re denotes the real part, x_1 and x_3 are defined in (3.4) and (2.1), and ϵ_{2d}, δ_{3d} and δ_{02} are given in (3.13). The scaled coordinates X and Z are real to the required level of approximation, but we allow the modal amplitudes A_0 and A to be complex. The mean flow correction term in (4.1) is induced by nonlinear effects in the critical layer.

As in G&L, Mankbadi *et al.* (1993) and Wu (1993), the mean flow $U(y, x_3)$ can be written as, when $r > 1$,

$$U = U_B + \sigma^{r-1}\bar{U}_p \quad \text{for} \quad y = O(1), \tag{4.5}$$

where U_B is the Blasius velocity and $\sigma^{r-1}\bar{U}_p$ is a small correction due to a pressure gradient. As y approaches the wall, which is assumed to be located at $y = 0$,

$$U_B \to \tau_0 y - \frac{\tau_0^2}{2 \times 4!}y^4 + \frac{11\tau_0^3}{4 \times 7!}y^7 + \ldots, \quad \bar{U}_p \to \bar{\mu}\left(-\bar{\tau}y + \tfrac{1}{2}y^2 + \ldots\right), \tag{4.6}$$

where the constant $\tau_0 (\simeq 0.332)$ denotes the scaled Blasius skin friction and $\bar{\mu}$ is defined in (3.3). The total wall-shear stress τ_w can be written as (Wundrow *et al.* 1994)

$$\tau_w = \tau_0 - \sigma^{r-1}\bar{\mu}\bar{\tau}. \tag{4.7}$$

The second term in (4.7) becomes $O(1)$ when $r = 1$, and (4.5) and (4.6) can then be rewritten as $U \to \tau_w y + (\bar{\mu}/2)y^2 + \ldots$ as $y \to 0$, as in Wu (1993).

The mode shapes Φ_0 and Φ satisfy Rayleigh's equations to the required levels of approximation

$$(U - \hat{c})(\mathrm{D}^2 - \hat{\gamma}^2)\hat{\Phi} - U''\hat{\Phi} = 0, \tag{4.8}$$

and the 'complex' wavenumbers α and γ and phase speeds c_0 and c are given to the required order of approximation, by

$$\hat{\gamma} = \sigma\left[\hat{\bar{\gamma}} + \sigma^r \frac{\bar{\alpha}\hat{A}'}{\mathrm{i}k\hat{\bar{\gamma}}\hat{A}}\right], \tag{4.9}$$

$$\hat{c} = \frac{\sigma\bar{c}}{1 + \sigma^r k\hat{A}'/(\mathrm{i}\bar{\alpha}\hat{A})}, \tag{4.10}$$

where the prime denotes differentiation with respect to the relevant argument, $\mathrm{D} \equiv \partial/\partial y$, and $\{\hat{A}, \hat{\Phi}, \hat{c}, \hat{\gamma}, \hat{\bar{\gamma}}, k\}$ can denote either $\{A_0, \Phi_0, c_0, \alpha, \bar{\alpha}, 1\}$ for the two-dimensional wave or $\{A, \Phi, c, \gamma, \bar{\gamma}, 2\}$ for the oblique modes.

The scaled velocity components $\tilde{U}$ and $\tilde{W}$ can be expressed in terms of Φ and $\mathrm{D}\Phi$ as shown in G&L, and $\bar{\gamma}$ and the propagation angle of the oblique modes $\pm\theta$ are defined as

$$\bar{\gamma} \equiv \left[(\bar{\alpha}/2)^2 + \bar{\beta}^2\right]^{1/2} \quad \text{and} \quad \theta \equiv \sin^{-1}(\bar{\beta}/\bar{\gamma}). \tag{4.11}$$

The scaled Strouhal number, $\bar{s}$, which is a real constant, of the two-dimensional fundamental mode is given by

$$\bar{s} = \bar{\alpha}\bar{c}. \tag{4.12}$$

Finally, Φ_0 and Φ must satisfy the boundary condition

$$\hat{\Phi} = 0 \quad \text{at} \quad y = 0, \tag{4.13}$$

for tangential flow near the wall.

Since we need only know the logarithmic derivative of $\hat{\Phi}$ the most convenient solution turns out to be the one given by Miles (1962), which is obtained by transforming (4.8) into a Riccati equation. It can be written as

$$\frac{\mathrm{D}\hat{\Phi}}{\hat{\Phi}} = \frac{U'}{U - \hat{c}} - \frac{1}{(U - \hat{c})^2\Omega^*}, \tag{4.14}$$

where

$$\Omega^* = 1/[\hat{\gamma}(1 - \hat{c})^2] + \Omega_0 + \hat{\gamma}\Omega_1 + \hat{\gamma}^2\Omega_2 + \ldots, \tag{4.15}$$

and Ω_0, Ω_1 and Ω_2 are the same as equations (3.4)–(3.6) of G&L.

Matching is simplified by using the classical 'inviscid function' (Lin 1955)

$$\hat{W} \equiv \frac{\hat{c}\mathrm{D}\hat{\Phi}}{U'\hat{\Phi} - (U-\hat{c})\mathrm{D}\hat{\Phi}}. \tag{4.16}$$

As in G&L, substituting the Miles' (1962) solution (4.14) and (4.15) along with (4.9) and (4.10) into (4.16), expanding for small σ, and finally using (4.5) to (4.7), we obtain

$$\begin{aligned}\hat{W} = {} & \frac{\bar{c}U'}{\hat{\bar{\gamma}}(1-\sigma\bar{c})^2} - \frac{\sigma\bar{c}\tau_w}{(1-\sigma\bar{c})^4}\left(J_1 + \sigma 2\bar{c}J_2 + \sigma^2\bar{c}^2J_3 + \frac{y^2}{8\tau_w}\right) \\ & + \sigma^2\hat{\bar{\gamma}}\bar{c}\tau_w\left(2J_4 + \sigma\bar{c}J_5 - \frac{\bar{c}y}{4\hat{\bar{\gamma}}\tau_w^2}\right) - \sigma^3\frac{7\bar{c}^3}{48\tau_w^2} + \sigma^r\frac{\bar{c}}{\tau_w^2}\left(\frac{3\bar{\mu}}{2} + \bar{\mu}_c\ln y\right) \\ & + \sigma^r\frac{\mathrm{i}\bar{c}\tau_w}{\hat{\bar{\gamma}}^2}\left(\frac{\bar{\alpha}}{k\hat{\bar{\gamma}}} + \frac{k\hat{\bar{\gamma}}}{\bar{\alpha}}\right)\frac{\hat{A}'}{\hat{A}} + \ldots,\end{aligned} \tag{4.17}$$

where

$$\bar{\mu}_c \equiv \bar{\mu} - \sigma^{3-r}(\tau_0 Y_c/2)^2, \tag{4.18}$$

the constants J_1 to J_5 are given in Appendix A and we have used the fact that

$$\bar{c} = \tau_w Y_c + \ldots. \tag{4.19}$$

5. The Tollmien region (inviscid wall layer)

The analyses of Graebel (1966) and Nield (1972) suggest that the scaled transverse coordinate

$$Y \equiv y/\sigma \tag{5.1}$$

must be introduced directly into (4.8) before attempting to obtain the solution. The solution that satisfies the boundary condition (4.13) is of the form

$$\hat{\Phi} = \sigma(\tau_w + \sigma\hat{a}^\dagger)Y + \sigma^{r+1}F(Y,\hat{\phi}) + \ldots, \tag{5.2}$$

where $\hat{a}^\dagger$, which can denote either $a_0^\dagger$ or $a^\dagger$ for two-dimensional or oblique modes respectively, is an order-one constant, and F, which can be discontinuous across Y_c, is given by

$$F^{\pm}(Y,\hat{\phi}) = f(Y) + \mathrm{i}\bar{\mu}_c Y_c[(Y-Y_c)\hat{\phi}^{\pm} + Y_c\hat{\phi}^{-}], \qquad Y \gtrless Y_c, \tag{5.3}$$

where

$$f(Y) = \bar{\mu}_c\left\{\tfrac{1}{2}Y^2 + Y_c[(Y-Y_c)\ln|Y-Y_c| + Y_c\ln Y_c]\right\} - \sigma^{3-r}\tau_0^2Y^3(Y_c + \tfrac{1}{2}Y)/4!, \tag{5.4}$$

and the integration constant $\hat{\phi}^{\pm}$ is, in general, a complex function of x_1.

Inserting (4.5)–(4.7) and (5.1)–(5.3) into (4.16) and re-expanding, we obtain

$$\hat{W} = \frac{U'}{\tau_w} + \sigma^r\frac{\bar{\mu}_c Y_c}{\tau_w}\left(\ln\frac{Y-Y_c}{Y_c} - \mathrm{i}\Delta\hat{\phi}\right) - \sigma^3\frac{\tau_w Y_c}{8}Y(2Y_c + Y) + \ldots, \tag{5.5}$$

for $Y > Y_c$, where $\Delta\hat{\phi}$ denotes either $\phi_0^- - \phi_0^+$ or $\phi^- - \phi^+$ for the two-dimensional or oblique modes, respectively.

Matching (5.5) with (4.17) shows that

$$1 = \frac{\bar{c}\tau_w}{\bar{\gamma}(1-\sigma\bar{c})^2} - \frac{\sigma\bar{c}\tau_w}{(1-\sigma\bar{c})^4}\left(J_1 + \sigma 2\bar{c}J_2 + \sigma^2\bar{c}^2J_3\right) + \sigma^2\bar{\gamma}\bar{c}\tau_w\left(2J_4 + \sigma\bar{c}J_5\right)$$
$$-\sigma^3\frac{7\bar{c}^3}{48\tau_w^2} + \sigma^r\frac{3\bar{c}\bar{\mu}}{2\tau_w^2} + \sigma^r(\ln\sigma + \ln Y_c)\frac{\bar{\mu}_c\bar{c}}{\tau_w^2} + \ldots, \tag{5.6}$$

$$\left(\cos\theta + \frac{1}{\cos\theta}\right)\frac{A'}{A} = -\frac{\bar{\mu}_c\bar{\gamma}^2Y_c}{\bar{c}\tau_w^2}\Delta\phi, \tag{5.7}$$

and

$$\frac{A_0'}{A_0} = -\frac{\bar{\mu}_c\bar{\alpha}^2Y_c}{2\bar{c}\tau_w^2}\Delta\phi_0 + \mathrm{i}\kappa_i, \tag{5.8}$$

where we have put

$$\bar{\gamma} = \bar{\alpha} + \sigma^r 2\kappa_i. \tag{5.9}$$

The scaled initial wavenumber detuning κ_i can be given arbitrarily as an initial condition. It follows from (4.11) and (5.9) that

$$\bar{\beta} = (\sqrt{3}/2)\bar{\alpha} + \sigma^r(4/\sqrt{3})\kappa_i + \ldots. \tag{5.10}$$

Equation (5.6) is the dispersion relation which, along with (5.9), determines $\bar{\gamma}$ and $\bar{\alpha}$ in terms of $\bar{c}$ or in terms of the scaled Strouhal number $\bar{s}$ which is defined in (4.12). Since its coefficients are all real, it is consistent with our original assertion that $\bar{\alpha}$ and $\bar{c}$ are real quantities. It also shows that $\bar{\gamma}$ possesses a power-series expansion of the form

$$\bar{\gamma} = \bar{\gamma}_0 + \sigma\bar{\gamma}_1 + \sigma^2\bar{\gamma}_2 + \sigma^3(\ln\sigma)\bar{\gamma}_{3l} + \sigma^3\bar{\gamma}_3 + \ldots + \sigma^r(\ln\sigma)\bar{\gamma}_{rl} + \sigma^r\bar{\gamma}_r + \ldots, \tag{5.11}$$

with similar expansions for $\bar{\alpha}$, $\bar{\beta}$ and $\bar{c}$. Equation (5.6) shows that $\bar{c}_0$ and $\bar{\gamma}_0$ satisfy the usual long-wavelength small-growth-rate dispersion relation

$$\bar{c}_0 = \bar{\gamma}_0/\tau_w. \tag{5.12}$$

Equations (5.7) and (5.8) relate the growth rates of the instability waves A'/A and A_0'/A_0 to the phase jumps $\Delta\phi$ and $\Delta\phi_0$ across the critical layer. To determine these latter quantities, it is necessary to consider the flow within the critical layer itself.

Equations (4.1)–(4.3), (4.7), (4.11) and (5.2)–(5.4) show that, as in G&L,

$$u = \sigma\tau_wY + \sigma^{r+1}\frac{\bar{\mu}}{2}Y^2 - \sigma^4\frac{\tau_0^2}{2\times 4!}Y^4 + \epsilon_{2d}\mathrm{Re}\left[\tau_w + \sigma a_0^\dagger + \sigma^r\left(f_{_Y} + \mathrm{i}\bar{\mu}_cY_c\phi_0^\pm\right)\right]A_0\mathrm{e}^{\mathrm{i}X}$$
$$+\delta_{3d}2\sec\theta\mathrm{Re}\left\{(\tau_w + \sigma a^\dagger)(1+\zeta\sin^2\theta) + \sigma^r\frac{\tau_w\zeta}{\bar{c}}\sin^2\theta\left[f + \frac{\bar{\mu}}{2}Y^2(1-\zeta)\right.\right.$$
$$-\frac{\tau_0^2Y^4}{2\times 4!}(3-\zeta) + \frac{\bar{c}f_{_Y}}{\tau_w\zeta\tan^2\theta} - \frac{\bar{c}A'}{\mathrm{i}\bar{\gamma}A}\left(\cos\theta + \frac{\tau_w^2Y^2\zeta}{\bar{c}^2\cos\theta}\right)$$
$$\left.\left.+\frac{\mathrm{i}\bar{c}\bar{\mu}_cY_c}{\tau_w}\left(\phi^- + \frac{\phi^\pm}{\zeta\sin^2\theta}\right)\right]\right\}A\mathrm{e}^{\mathrm{i}X/2}\cos Z + \delta_{02}\mathrm{Re}\,\bar{U}_{02}(Y_{c\pm}, x_1)\mathrm{e}^{2\mathrm{i}Z} + \ldots, \tag{5.13}$$

$$v = -\sigma^2\tau_wY\,\mathrm{Re}\left[\epsilon_{2d}\mathrm{i}\bar{\alpha}A_0\mathrm{e}^{\mathrm{i}X} + \delta_{3d}2\mathrm{i}\bar{\gamma}A\mathrm{e}^{\mathrm{i}X/2}\cos Z\right] + \ldots, \tag{5.14}$$

$$w = -\delta_{3d}2\sin\theta\mathrm{Re}\,\mathrm{i}\tau_w\zeta A\mathrm{e}^{\mathrm{i}X/2}\sin Z + \ldots, \tag{5.15}$$

$$p = P + \sigma\bar{c}\tau_w\mathrm{Re}\left[\epsilon_{2d}A_0\mathrm{e}^{\mathrm{i}X} + \delta_{3d}2\cos\theta A\mathrm{e}^{\mathrm{i}X/2}\cos Z\right] + \ldots, \tag{5.16}$$

where $\bar{U}_{02}$ is the wall-layer expansion corresponding to $\tilde{U}_{02}$ in (4.1), P denotes the mean pressure at the critical level, and we have put

$$\zeta \equiv \bar{c}/(\tau_w Y - \bar{c}). \tag{5.17}$$

Since these solutions become singular at the critical level $Y = Y_c$, they have to be rescaled in this region.

6. The critical level

As in Goldstein *et al.* (1987), G&L, and others, the thickness of the small-growth-rate non-equilibrium critical layer must be of the same order as the growth rate, i.e. $O(\sigma^{r+1})$ in the present case, in order to make the growth rate and the linear convection terms of the same order of magnitude there. The appropriate transverse coordinate in this region, which was given in (3.14) can be rewritten as

$$\bar{\eta} = (Y - Y_c)/\sigma^r = (y - y_c)/\sigma^{r+1}. \tag{6.1}$$

The viscous parameter λ is defined in (3.12). The measures of the instability wave amplitudes ϵ_{2d} and δ_{3d} and the magnitude of the mean flow correction term δ_{02} are given in (3.13).

The governing equations expressed in terms of the scaled variables x_1, X, Z and $\bar{\eta}$ are

$$\bar{\mathrm{D}}\{u, \bar{v}, w\} = -\left\{\bar{\alpha} p_X + \sigma^r p_{x_1}, \sigma^{-2r-4} p_{\bar{\eta}}, \bar{\beta} p_Z\right\}, \tag{6.2}$$

$$\bar{\alpha} u_X + \bar{v}_{\bar{\eta}} + \bar{\beta} w_Z + \sigma^r u_{x_1} = 0, \tag{6.3}$$

where we have put

$$\bar{\mathrm{D}} \equiv \bar{\alpha}(u - \sigma\bar{c})\frac{\partial}{\partial X} + \bar{v}\frac{\partial}{\partial \bar{\eta}} + \bar{\beta} w \frac{\partial}{\partial Z} + \sigma^r u \frac{\partial}{\partial x_1} - \sigma^{r+1}\lambda \frac{\partial^2}{\partial \bar{\eta}^2}, \tag{6.4}$$

and

$$v = \sigma^{r+2}\bar{v}. \tag{6.5}$$

Introducing (3.13) and (6.1) into (5.13)–(5.16) and re-expanding the result for small $\bar{\eta}$ shows that the critical-layer solution should be of the form

$$u - \sigma\bar{c} = \sigma^{r+1}\tau_w \bar{\eta} + \sigma^{2r+1}u^{(1)} + \sigma^{3r+1}u^{(2)} + \sigma^{4r+1}u^{(3)} + \sigma^{5r+1}u^{(4)} + \ldots, \tag{6.6}$$

$$\bar{v} = -\sigma^{2r+1} 2\bar{\gamma}\tau_w Y_c \mathrm{Re}\mathrm{i}A\mathrm{e}^{\mathrm{i}X/2}\cos Z + \sigma^{3r+1}\bar{v}^{(2)} + \sigma^{4r+1}\bar{v}^{(3)} + \sigma^{5r+1}\bar{v}^{(4)} + \ldots, \tag{6.7}$$

$$w = \sigma^{2r+1}w^{(1)} + \sigma^{3r+1}w^{(2)} + \sigma^{4r+1}w^{(3)} + \sigma^{5r+1}w^{(4)} + \ldots, \tag{6.8}$$

$$p = P + \sigma^{3r+2}(2\bar{c}\tau_w \cos\theta)\mathrm{Re}A\mathrm{e}^{\mathrm{i}X/2}\cos Z + \sigma^{4r+2}p^{(2)} + \sigma^{5r+2}p^{(3)} + \ldots. \tag{6.9}$$

Substituting the expansions (6.6)–(6.9) into (6.2)–(6.5) with (4.7) we can obtain the governing equations for $u^{(l)}$, $\bar{v}^{(l)}$, $w^{(l)}$ and $p^{(l)}$ which are the same as equations (5.14)–(5.21) and Appendix A of G&L with their U_0' replaced by τ_w.

We must now solve these equations subject to the transverse boundary condition that they match onto the outer solution (5.13)–(5.16); this is the same as the boundary value problem in G&L. The following normalized variables are introduced:

$$\tilde{x} = \tfrac{1}{2}\tau_w \bar{\alpha} x_1 - x_0, \quad \eta = \bar{\eta}/\bar{c}, \quad \bar{\lambda} = 2\lambda/(\tau_w \bar{\alpha}\bar{c}^3), \tag{6.10}$$

where x_0 is a coordinate origin shift, to be chosen subsequently.

The relevant solutions are given by

$$\left\{u^{(1)} - \bar{c}\bar{\mu}_c^{\dagger} Y_c \eta, w^{(1)}\right\} = 2\mathrm{Re}\left\{\mathrm{i}\tan\theta\cos Z, \sin Z\right\} Q^{(1)}(\eta, \tilde{x})\mathrm{e}^{\mathrm{i}X/2}, \tag{6.11}$$

for the lowest-order and by

$$\left\{u_\eta^{(l)} - Q_M^{(l)}, \bar{v}^{(l)}, w^{(l)}\right\} = \mathrm{Re}\sum_{n,m}\left\{Q_{n,m}^{(l)}(\eta, \tilde{x}), V_{n,m}^{(l)}(\eta, \tilde{x}), W_{n,m}^{(l)}(\eta, \tilde{x})\right\}\mathrm{e}^{\mathrm{i}(nX/2+mZ)}, \tag{6.12}$$

for $l = 2, 3$ and 4, where

$$\bar{\mu}_c^{\dagger} \equiv \bar{\mu} - \sigma^{3-r}\tfrac{1}{3}(\tfrac{1}{2}\tau_0 Y_c)^2, \tag{6.13}$$

$$Q_M^{(2)} = (\bar{\mu} - \sigma^{3-r}\tfrac{1}{4}\bar{c}^2)\bar{c}^2\eta + \ldots, \quad Q_M^{(3)} = -\sigma^{6-2r}\tfrac{1}{4}\bar{c}^3\tau_w^2 Y_c\eta^2 + \ldots, \tag{6.14}$$

and the governing equations and boundary conditions for $Q^{(1)}$, $Q_{n,m}^{(l)}$, $V_{n,m}^{(l)}$, and $W_{n,m}^{(l)}$ are the same as equations (5.27)–(5.29), (5.35)–(5.40) and Appendix B of G&L. Matching with the outer solution (5.14) shows that

$$V_{2,0}^{(2)} \to -\mathrm{i}\tau_w Y_c \bar{\alpha} A_0 \quad \text{as} \quad \eta \to \pm\infty. \tag{6.15}$$

Before attempting to solve these equations, it is convenient to introduce the following normalized variables:

$$\bar{x} = \hat{\kappa}\tilde{x}, \quad \tilde{\eta} = \eta/\hat{\kappa}, \quad \tilde{\bar{\lambda}} = \bar{\lambda}/\hat{\kappa}^3, \quad \tilde{X} = X - X_0, \tag{6.16}$$

$$\tilde{A} = (Y_c M)^{1/2}/(\bar{c}\hat{\kappa}^3)A\mathrm{e}^{\mathrm{i}X_0/2}, \quad \tilde{A}_0 = (M/\hat{\kappa}^4)A_0\mathrm{e}^{\mathrm{i}X_0}, \tag{6.17}$$

where

$$M = 8\pi Y_c\bar{\beta}^2/(\tau_w^3\bar{\alpha}\bar{c}^3), \tag{6.18}$$

$\hat{\kappa}$ is a normalization parameter which can be chosen arbitrarily and X_0 is the coordinate origin shift to be chosen subsequently. The equations, which we refer to as the critical-layer equations, now become

$$\mathscr{L}_1\tilde{Q}^{(1)} = \tilde{A}, \tag{6.19}$$

$$\mathscr{L}_1\tilde{q}_{1,1}^{(3L)} = 2\mathrm{i}(\kappa_0/\hat{\kappa})\tilde{A}, \tag{6.20}$$

$$\mathscr{L}_2\tilde{Q}_{2,0}^{(4L)} = 4\mathrm{i}(\kappa_0/\hat{\kappa})\tilde{A}_0, \tag{6.21}$$

$$\mathscr{L}_n\left\{\tilde{Q}_{n,m}^{(l)}, \tilde{W}_{n,m}^{(l)}, \tilde{q}_{n,1}^{(3)}\right\} = \left\{G_{n,m}^{(l)}, H_{n,m}^{(l)}, R_{n,1}^{(3)}\right\}, \tag{6.22}$$

$$\tilde{U}_{n,m\tilde{\eta}}^{(l)} = \tilde{Q}_{n,m}^{(l)}, \tag{6.23}$$

$$\tilde{V}_{0,2\tilde{\eta}}^{(2)} = 2\tilde{W}_{0,2}^{(2)}, \quad \tilde{V}_{2,0\tilde{\eta}}^{(2)} = 2\tilde{U}_{2,0}^{(2)}, \quad \tilde{V}_{1,1\tilde{\eta}\tilde{\eta}}^{(3)} = \tilde{q}_{1,1}^{(3)}, \quad \tilde{V}_{3,1\tilde{\eta}\tilde{\eta}}^{(3)} = 3\tilde{q}_{3,1}^{(3)}, \tag{6.24}$$

for $l = 2, 3$ and 4, where we have put

$$\mathscr{L}_n \equiv \partial/\partial\bar{x} + \mathrm{i}n\tilde{\eta} - \tilde{\bar{\lambda}}\partial^2/\partial\tilde{\eta}^2, \tag{6.25}$$

$$\tilde{q}_{1,1}^{(3)} + \tilde{q}_{1,1}^{(3L)} \equiv \tilde{Q}_{1,1}^{(3)} + \tilde{W}_{1,1\tilde{\eta}}^{(3)} - \mathrm{i}\tilde{Q}_{1,1\bar{x}}^{(2)}, \quad \tilde{q}_{3,1}^{(3)} \equiv \tilde{Q}_{3,1}^{(3)} + \tfrac{1}{3}\tilde{W}_{3,1\tilde{\eta}}^{(3)}, \tag{6.26}$$

and

$$\kappa_0 \equiv \pi(\bar{\mu} - \sigma^{3-r}\tfrac{1}{4}\bar{c}^2)Y_c\bar{\alpha}/(\tau_w^3\bar{c}) \tag{6.27}$$

is the linear growth rate of the two-dimensional wave. The normalized variables $\tilde{Q}^{(1)}$, $\tilde{Q}_{n,m}^{(l)}$, $\tilde{Q}_{2,0}^{(4L)}$, and $\tilde{W}_{n,m}^{(l)}$ of $Q^{(l)}$, $Q_{n,m}^{(l)}$, $Q_{2,0}^{(4L)}$, and $W_{n,m}^{(l)}$ respectively, are defined in Appendix B along with $G_{n,m}^{(l)}$, $H_{n,m}^{(l)}$, and $R_{n,1}^{(3)}$. The $\tilde{V}_{2,0}^{(2)}$ in (6.24) is the normalized

variable corresponding to $V_{2,0}^{(2)} + \mathrm{i}\tau_w Y_c \bar{\alpha} A_0$ (see (6.15)). Equations (6.19)–(6.22) must be solved subject to the transverse boundary conditions

$$\tilde{Q}^{(1)}, \tilde{q}_{1,1}^{(3L)}, \tilde{Q}_{2,0}^{(4L)}, \tilde{Q}_{n,m}^{(l)}, \tilde{W}_{n,m}^{(l)}, \tilde{q}_{n,1}^{(3)} \to 0 \quad \text{as} \quad \tilde{\eta} \to \pm\infty, \tag{6.28}$$

for $l = 2, 3$ and 4.

The critical-layer equations (6.20) and (6.21) for the linear problem can be solved by taking Fourier transforms with respect to $\tilde{\eta}$ and integrating the results with respect to $\bar{x}$. The solutions are

$$\tilde{q}_{1,1}^{(3L)} = 2\mathrm{i}\frac{\kappa_0}{\hat{\kappa}} \mathrm{e}^{-\mathrm{i}\tilde{\eta}\bar{x}} \int_{-\infty}^{\bar{x}} \mathrm{e}^{\mathrm{i}\tilde{\eta}\tilde{x} - \tilde{\lambda}(\bar{x}-\tilde{x})^3/3} \tilde{A}(\tilde{x}) \mathrm{d}\tilde{x}, \tag{6.29}$$

$$\tilde{Q}_{2,0}^{(4L)} = 4\mathrm{i}\frac{\kappa_0}{\hat{\kappa}} \mathrm{e}^{-2\mathrm{i}\tilde{\eta}\bar{x}} \int_{-\infty}^{\bar{x}} \mathrm{e}^{2\mathrm{i}\tilde{\eta}\tilde{x} - 4\tilde{\lambda}(\bar{x}-\tilde{x})^3/3} \tilde{A}_0(\tilde{x}) \mathrm{d}\tilde{x}. \tag{6.30}$$

The linear velocity jumps across the critical layer are obtained by integrating (6.29) and (6.30) with respect to $\tilde{\eta}$,

$$\int_{-\infty}^{\infty} \tilde{q}_{1,1}^{(3L)} \mathrm{d}\tilde{\eta} = 2\pi\mathrm{i}\frac{\kappa_0}{\hat{\kappa}} \tilde{A}(\bar{x}), \tag{6.31}$$

$$\int_{-\infty}^{\infty} \tilde{Q}_{2,0}^{(4L)} \mathrm{d}\tilde{\eta} = 2\pi\mathrm{i}\frac{\kappa_0}{\hat{\kappa}} \tilde{A}_0(\bar{x}). \tag{6.32}$$

The solutions of the critical-layer equations have to match onto the discontinuous $O(\delta_{3d}\sigma^r) = O(\sigma^{4r+1})$ and $O(\epsilon_{2d}\sigma^r) = O(\sigma^{5r+1})$ terms (see (3.13)) in (5.13) for the oblique and two-dimensional modes respectively. It therefore follows from (5.7), (5.8), (6.6), (6.12) and (6.26) along with (6.31) and (6.32) that these solutions must satisfy

$$\left(\cos\theta + \frac{1}{\cos\theta}\right)\left(\frac{\mathrm{d}\tilde{A}}{\mathrm{d}\bar{x}} - \frac{\kappa_{ob}}{\hat{\kappa}}\tilde{A}\right) = -\frac{\mathrm{i}}{4\pi\cos^2\theta} \int_{-\infty}^{\infty} \tilde{q}_{1,1}^{(3)} \mathrm{d}\tilde{\eta}, \tag{6.33}$$

$$\frac{\mathrm{d}\tilde{A}_0}{\mathrm{d}\bar{x}} - \left(\frac{\kappa_0}{\hat{\kappa}} + \mathrm{i}\bar{\kappa}_i\right)\tilde{A}_0 = -\frac{\mathrm{i}}{2\pi} \int_{-\infty}^{\infty} \tilde{Q}_{2,0}^{(4)} \mathrm{d}\tilde{\eta}, \tag{6.34}$$

where the linear growth rate of the oblique mode κ_{ob} and the effective wavenumber detuning $\bar{\kappa}_i$ (which corresponds to $\tilde{\kappa}_i$ of G&L in their final amplitude equation (5.51)) are defined as

$$\kappa_{ob} = \kappa_0/[2\cos\theta(1 + \cos^2\theta)], \tag{6.35}$$

$$\bar{\kappa}_i = \frac{2\kappa_i}{\hat{\kappa}\tau_w\bar{\alpha}}. \tag{6.36}$$

These equations ultimately determine the unknown instability wave amplitudes $\tilde{A}$ and $\tilde{A}_0$. They arise from the requirement that the change in the subharmonic and fundamental components of the velocity fluctuation across the critical layer as calculated from the external solutions are the same as when they are calculated from the internal solutions.

The system of equations (6.19) and (6.22)–(6.24) along with the jump conditions (6.33) and (6.34) are the final equations to be solved subject to the transverse boundary conditions (6.28) and upstream boundary condition. The variables are normalized in such a way that the nonlinear equations (6.19) and (6.22)–(6.24) do not include the basic mean-flow-dependent parameters, τ_w, $\bar{\mu}$, $\bar{c}$, $\bar{\alpha}$, $\bar{\gamma}$, $\tilde{\lambda}$, etc., explicitly and only the linear growth rates are mean flow dependent. It is easy to show that $\tilde{\lambda}$ in (6.25)

becomes unity when $\hat{\kappa}$ is equal to $\bar{\lambda}^{1/3}$ from (6.16). We kept the obliqueness angle θ arbitrary in deriving these equations so that they would apply for any obliqueness angle when only a pair of oblique modes enters the interaction. The linear growth rates κ_0 and κ_{ob} in (6.27) and (6.35) become negligibly small when $\bar{\mu} \ll 1$ and $1 \leqslant r < 3$.

As mentioned earlier, the upstream flow can start as a resonant triad of linear instability waves as in G&L or as a resonant triad of linear and nonlinear instability waves as in Wundrow *et al.* (1994) and Goldstein (1994). The upstream boundary condition for the former case becomes

$$\tilde{A} \to a^{(0)} \mathrm{e}^{(\kappa_{ob}/\hat{\kappa})\bar{x}}, \quad \tilde{A}_0 \to \mathrm{e}^{(\kappa_0/\hat{\kappa}+\mathrm{i}\bar{\kappa}_i)\bar{x}} \quad \text{as} \quad \bar{x} \to -\infty, \tag{6.37}$$

where

$$a^{(0)} = \frac{Y_c^{1/2}}{\hat{\kappa}\bar{c}} \frac{A^{(0)}}{(A_0^{(0)})^{1/2}} \left(\frac{\hat{\kappa}^4}{M|A_0^{(0)}|} \right)^{[\kappa_{ob}-(\kappa_0+\mathrm{i}\bar{\kappa}_i\hat{\kappa})/2]/\kappa_0} \tag{6.38}$$

and $A^{(0)}$ and $A_0^{(0)}$ are the complex scaled initial amplitudes of the instability waves, i.e.

$$A \to A^{(0)} \mathrm{e}^{\kappa_{ob}\tau_w\bar{\alpha}x_1/2}, \quad A_0 \to A_0^{(0)} \mathrm{e}^{(\kappa_0+\mathrm{i}\bar{\kappa}_i\hat{\kappa})\tau_w\bar{\alpha}x_1/2} \quad \text{as} \quad x_1 \to -\infty. \tag{6.39}$$

The origin shifts x_0 and X_0 in (6.10) and (6.16) are chosen to satisfy

$$(M/\hat{\kappa}^4) A_0^{(0)} \mathrm{e}^{\mathrm{i}X_0+(\kappa_0+\mathrm{i}\bar{\kappa}_i\hat{\kappa})x_0} = 1. \tag{6.40}$$

The upstream conditions for the resonant triad of linear/nonlinear waves can be given as solutions of the preceding linear or nonlinear stages as was shown in Wundrow *et al.* (1994) and Goldstein (1994). The upstream condition for the non-equilibrium critical-layer stage of a Blasius boundary layer is given by (9.3) below.

Finally, (4.11), (5.6), (5.9), (5.10) and (6.35) show that

$$\bar{\alpha} = \bar{\gamma}, \quad \cos\theta = \tfrac{1}{2}, \quad \bar{c} = \bar{\alpha}/\tau_w = \tau_w Y_c, \quad \kappa_{ob} = \tfrac{4}{5}\kappa_0, \tag{6.41}$$

to the order of approximation of the analysis.

7. Numerical method

The critical-layer equations (6.19) and (6.22)–(6.24) together with the jump conditions (6.33) and (6.34) (along with the relation (6.41)) subject to the transverse boundary conditions (6.28) and upstream condition can be solved both numerically and analytically. The numerical method will be presented in this section and the analytical solution will be summarized in the following section.

The system of partial differential equations (6.19) and (6.22) is solved by using the Crank–Nicolson method with the Thomas algorithm (see Anderson, Tannehill & Pletcher 1984). Newton and Cotes' integration formula of high (up to eighth) order (see Kopal 1961, pp. 575–577) is used to compute the integrals of (6.23) and (6.24). Equations (6.33) and (6.34) are solved by using a predictor-corrector method where a fifth-order Adams–Bashforth method was used for the predictor step and variable (up to twelfth)-order Adams–Moulton method was used for the corrector step (see Gear 1971, pp. 110–113).

We use a uniform step size (of typical value of $\Delta\bar{x} = 0.002$) for the streamwise marching. However, a transformation is used for the transverse coordinate $\tilde{\eta}$ in order to have a refined mesh near $\tilde{\eta} = 0$. A suitable transformation which maps the original non-uniform grid $\Delta\tilde{\eta}$, with $-H \leqslant \tilde{\eta} \leqslant H$, into the computational uniform grid $\Delta\tilde{y}$,

where $-1 \leqslant \tilde{y} \leqslant 1$, is given by (see Anderson *et al.* 1984, pp. 250–251)

$$\tilde{y} = (1/\hat{\tau}) \sinh^{-1}[(\tilde{\eta} \sinh \hat{\tau})/H], \tag{7.1}$$

where $\hat{\tau}$ is the stretching parameter which varies from zero (no stretching) to large values (refinement near $\tilde{\eta} = 0$). It is easy to obtain the metrics $\mathrm{d}\tilde{y}/\mathrm{d}\tilde{\eta}$ and $\mathrm{d}^2\tilde{y}/\mathrm{d}\tilde{\eta}^2$ from (7.1) and incorporate them into the Crank–Nicolson scheme. The values of the parameters that we used were $\hat{\tau} = 6$, $H = 200$ (for $\tilde{\lambda} = 1$) or $H = 4800$ (for $\tilde{\lambda} = 10^4$) and $\Delta\tilde{y} = 10^{-3}$.

Equation (6.19) implies that the asymptotic behaviour of $\tilde{Q}^{(1)}$ as $\tilde{\eta} \to \pm\infty$ is

$$\tilde{Q}^{(1)} \to -\mathrm{i}\tilde{A}/\tilde{\eta} + \tilde{A}_{\bar{x}}/\tilde{\eta}^2 + \ldots. \tag{7.2}$$

Similarly the asymptotic behaviour of $\tilde{Q}^{(l)}_{n,m}$, $\tilde{W}^{(l)}_{n,m}$, and $\tilde{q}^{(3)}_{n,1}$ as $\tilde{\eta} \to \pm\infty$ can be obtained from (6.22). These asymptotic solutions are used to give boundary values at $\tilde{\eta} = \pm H$ for (6.19) and (6.22) instead of the original transverse boundary conditions (6.28).

8. Amplitude equations and their viscous limit

The critical-layer equations (6.19), (6.22)–(6.24), (6.33) and (6.34) subject to (6.28) are solved analytically in Appendix C of G&L for the inviscid case with the parameters given by (6.41). The results show that the amplitudes $\tilde{A}$ and $\tilde{A}_0$ satisfy integro-differential equations. It is possible to modify the G&L analysis to include the viscosity as was done for special cases by Goldstein & Lee (1993), Wu *et al.* (1993) and Leib & Lee (1995), and in the general case by Wu (1995). To this end (6.19) can be solved to obtain

$$\tilde{Q}^{(1)} = \mathrm{e}^{-\mathrm{i}\tilde{\eta}\bar{x}} \int_{-\infty}^{\bar{x}} \mathrm{e}^{\mathrm{i}\tilde{\eta}\tilde{x} - \tilde{\lambda}(\bar{x}-\tilde{x})^3/3} \tilde{A}(\tilde{x}) \mathrm{d}\tilde{x}. \tag{8.1}$$

By substituting (8.1) along with other lower-order solutions into the right-hand side of (6.22) and taking Fourier transform with respect to $\tilde{\eta}$, we can successively solve $\tilde{Q}^{(l)}_{n,m}$, $\tilde{W}^{(l)}_{n,m}$, and $\tilde{q}^{(3)}_{n,1}$. We refer the reader to Wu (1995) for the detailed derivations. Here we merely note that substitution of the solutions into the jump conditions (6.33) and (6.34) shows that the amplitudes $\tilde{A}$ and $\tilde{A}_0$ satisfy the following integro-differential equations:

$$\left(\cos\theta + \frac{1}{\cos\theta}\right)\left(\frac{\mathrm{d}\tilde{A}}{\mathrm{d}\bar{x}} - \frac{\kappa_{ob}}{\hat{\kappa}}\tilde{A}\right) = \mathrm{i}\int_{-\infty}^{\bar{x}} K_1(\bar{x}|x_1)\tilde{A}_0(x_1)\tilde{A}^*(2x_1 - \bar{x})\mathrm{d}x_1 + \frac{\mathrm{i}}{4\cos^2\theta}\int_{-\infty}^{\bar{x}}\int_{-\infty}^{x_1} K_2(\bar{x}|x_1, x_2)\tilde{A}(x_1)\tilde{A}(x_2)\tilde{A}^*(x_1 + x_2 - \bar{x})\mathrm{d}x_2\mathrm{d}x_1, \tag{8.2}$$

$$\frac{\mathrm{d}\tilde{A}_0}{\mathrm{d}\bar{x}} - \left(\frac{\kappa_0}{\hat{\kappa}} + \mathrm{i}\bar{\kappa}_i\right)\tilde{A}_0 = \mathrm{i}\int_{-\infty}^{\bar{x}}\int_{-\infty}^{x_1}\Big[K_3(\bar{x}|x_1, x_2)\tilde{A}_0(x_1)\tilde{A}(x_2)\tilde{A}^*(2x_1 + x_2 - 2\bar{x}) + K_4(\bar{x}|x_1, x_2)\tilde{A}(x_1)\tilde{A}_0(x_2)\tilde{A}^*(x_1 + 2x_2 - 2\bar{x})\Big]\mathrm{d}x_2\mathrm{d}x_1 + \mathrm{i}\int_{-\infty}^{\bar{x}}\int_{-\infty}^{x_1}\int_{-\infty}^{x_2} K_5(\bar{x}|x_1, x_2, x_3)\tilde{A}(x_1)\tilde{A}(x_2)\tilde{A}(x_3)\tilde{A}^*(x_1 + x_2 + x_3 - 2\bar{x})\mathrm{d}x_3\mathrm{d}x_2\mathrm{d}x_1, \tag{8.3}$$

where the asterisks denote complex conjugates and we have used (4.19). These are generalized versions of the integro-differential equations given in G&L and Wu (1995). The scaling factor σ^{3-r} is now included in the linear growth rates κ_0 and κ_{ob}, as given

in (4.18), (6.27) and (6.35), and the viscous effect now appears in the kernel functions. We have also retained the obliqueness angle θ as a parameter. These equations determine the amplitudes of long-wavelength small-growth-rate instability waves in boundary layers whose critical layers are governed by non-equilibrium dynamics.

The kernel function K_1 of the parametric-resonance term is defined as (Goldstein & Lee 1993)

$$K_1 = \mathrm{e}^{-2\tilde{\lambda}(\bar{x}-x_1)^3/3}(\bar{x}-x_1)^2, \tag{8.4}$$

and K_2 for the self-interaction term, which was first derived by Wu *et al.* (1993), is given in Appendix C. It is easy to show that these viscous kernel functions K_1 and K_2 reduce to the corresponding inviscid kernel functions given in G&L in the limit $\tilde{\lambda} \to 0$. The formula for K_5 of the back-reaction term in the plane-wave amplitude equation is very complex and is given by Wu (1995) together with K_3 and K_4 for the mutual-interaction term. Rather than integrating the amplitude equations (8.2) and (8.3), we choose to directly solve the non-homogeneous partial differential equations with jump conditions by using the numerical method described in the previous section. However, it is easier to solve the amplitude equations when the mutual-interaction and back-reaction terms in the plane-wave amplitude equation are missing or unimportant, i.e. for the two oblique-mode interactions considered by Goldstein & Choi (1989), Wu *et al.* (1993) and Leib & Lee (1995).

As mentioned earlier, the normalization parameter $\hat{\kappa}$ in (6.16) can be chosen arbitrarily. The viscosity parameter can be eliminated from the kernel functions by choosing $\hat{\kappa} = \tilde{\lambda}^{1/3}$. This is very convenient for computation because evaluating the viscous kernel functions requires a considerable amount of computational time.

The numerical computations with finite viscosity, as given in §10, show that the solutions always develop a singularity at some finite value of $\bar{x}$, say $\bar{x}_s$, as was also observed in the inviscid limit by G&L. Then as $\bar{x} \to \bar{x}_s$, $\tilde{A}_{\bar{x}}$ and $\tilde{A}_{0\bar{x}}$ become large compared with $\tilde{A}$ and $\tilde{A}_0$ and are balanced by the integral terms on the right-hand sides of (8.2) and (8.3). As in G&L and Wu *et al.* (1993) the asymptotic form of the solution when $\bar{x} \to \bar{x}_s$ is given by

$$\tilde{A} = b/(\bar{x}_s - \bar{x})^{3+\mathrm{i}\psi}, \quad \tilde{A}_0 = b_0/(\bar{x}_s - \bar{x})^{4+2\mathrm{i}\psi}, \tag{8.5}$$

where $\bar{x}_s$ and ψ are real constants, b and b_0 are complex constants, and ψ, $|b|$, $|b_0|$ and the argument of b^2/b_0 can be determined from equations (6.7) and (6.8) of G&L.

The viscous limits of (8.2) and (8.3), which can be obtained by using the method described in Wu *et al.* (1993), are

$$\left(\cos\theta + \frac{1}{\cos\theta}\right)\left(\frac{\mathrm{d}\tilde{A}}{\mathrm{d}\bar{x}} - \frac{\kappa_{ob}}{\hat{\kappa}}\tilde{A}\right) = \frac{\mathrm{i}}{2\tilde{\lambda}}\tilde{A}_0(\bar{x})\tilde{A}^*(\bar{x}) - \frac{\mathrm{i}}{2\tilde{\lambda}^{4/3}}\left(\frac{1}{18}\right)^{1/3}(\tan^2\theta\cos 2\theta)\Gamma\left(\tfrac{1}{3}\right)\tilde{A}(\bar{x})\int_{-\infty}^{\bar{x}}|\tilde{A}(x_1)|^2\mathrm{d}x_1, \tag{8.6}$$

$$\frac{\mathrm{d}\tilde{A}_0}{\mathrm{d}\bar{x}} - \left(\frac{\kappa_0}{\hat{\kappa}} + \mathrm{i}\bar{\kappa}_i\right)\tilde{A}_0 = 0. \tag{8.7}$$

The derivation of (8.7) assumes that the viscous limits of the mutual-interaction and back-reaction terms in (8.3) are of higher-order in the viscous parameter $\tilde{\lambda}$. This can be proved from the full viscous amplitude equations given in Wu (1995). We must also add viscous correction terms, which are of higher-order terms in the present non-equilibrium analysis, to the linear growth rates κ_0 and κ_{ob} in (6.27) and (6.35) in order to make this solution valid for large values of $\tilde{\lambda}$ (G&L; Mankbadi *et al.* 1993;

Wu 1993). Mankbadi *et al.* (1993) and Wu (1993) derived these amplitude equations directly from the Navier–Stokes equations.

Equations (8.6) and (8.7) are invariant under the transform

$$\tilde{\lambda} \to \tilde{\lambda}_v/\sigma^r, \quad \tilde{A}_0 \to \tilde{A}_{0v}/\sigma^r, \quad \tilde{A} \to \tilde{A}_v/\sigma^{2r/3}. \tag{8.8}$$

The scaling of this viscous-limit problem can be obtained by putting (see (4.1) and (6.17))

$$\sigma^r\lambda \to \lambda_v \left[= 1/(\sigma^{2r+4}R_\Delta)\right], \quad \epsilon_{2d}/\sigma^r \to \epsilon_{2dv} \left[= \sigma^{3r+1}\right], \quad \delta_{3d}/\sigma^{2r/3} \to \delta_{3dv} \left[= \sigma^{7r/3+1}\right], \tag{8.9}$$

where λ, ϵ_{2d} and δ_{3d} are defined in (3.12) and (3.13), and $\lambda_v = \tau_w\bar{\alpha}\bar{c}^3\hat{\kappa}^3\tilde{\lambda}_v/2$ from (6.10) and (6.16).

The scalings in (8.9) can also be obtained directly from the generalized scaling (3.5)–(3.7) by taking $m = 0$. It is easy to show that the amplitude equations (8.6) and (8.7), with $\{\tilde{\lambda}, \tilde{A}, \tilde{A}_0\}$ replaced by $\{\tilde{\lambda}_v, \tilde{A}_v, \tilde{A}_{0v}\}$ and with the modified linear growth rates, and the scalings in (8.9) along with (3.2) to (3.4) are indeed the same as those obtained by Mankbadi *et al.* (1993) for the Blasius boundary layer if we put $r = 3$ and $\bar{\mu} = 0$ and those obtained by Wu (1993) for the favourable-pressure-gradient boundary layer when we take $r = 1$.

The scaling, which we discussed in §3, for a viscous (quasi-equilibrium) resonant-triad interaction in a boundary layer with small non-zero pressure gradient (i.e. larger viscous effect than in G&L or smaller pressure gradient than in Wu 1993) can also be recovered by putting $r = 3$ with order-one $\bar{\mu}$. The amplitudes are governed by (8.6) and (8.7) if their linear growth rates are modified to include the viscous Stokes-layer effects.

9. Blasius boundary layer

Goldstein (1994, 1995) studied the non-equilibrium critical-layer effects in a Blasius boundary layer. He showed that, when the initial amplitude of the oblique mode is exponentially small, the initial parametric resonance growth of quasi-equilibrium type is followed by the non-equilibrium-type interaction before the self-interaction becomes important. We will summarize the analysis which was first given by Goldstein (1994) in this section and give some relevant numerical results in the following section.

It is well known that the Reynolds number R_Δ scales like (wavenumber)$^{-10}$ (or σ^{-10}) in the upper-branch regime of a Blasius boundary layer (e.g. Reid 1965; Goldstein & Durbin 1986). The scaled viscous parameter λ defined in (3.12) will then be $O(1)$ in this region if we take

$$r = 2, \tag{9.1}$$

which implies from (3.4) and (3.13) that

$$x_1 = \sigma^3 x, \quad \epsilon_{2d} = \sigma^9, \quad \delta_{3d} = \delta_{02} = \sigma^7. \tag{9.2}$$

The scalings in (9.1) and (9.2) along with (3.2), (3.12) and (3.14), also in table 1, can be used for the non-equilibrium analysis of the later fully coupled stage in a Blasius boundary layer. From the generalized non-equilibrium analysis described in §§4–8, we can readily obtain the system of critical-layer equations (6.19), (6.22)–(6.24), (6.33) and (6.34) or the amplitude equations (8.2) and (8.3), with the parameter r is now given by (9.1).

Since $\bar{\mu}$ is zero for a Blasius boundary layer, $\bar{\mu}_c$, κ_0 and κ_{ob} in (4.18), (6.27) and (6.35) become $O(\sigma)$. We, of course, must add the effects of the viscous Stokes layer to

(6.27) and (6.35), as was given in Mankbadi *et al.* (1993), in order to be correct up to $O(\sigma)$. The linear growth rate terms are negligible in the jump conditions (6.33) and (6.34) and in the amplitude equations (8.2) and (8.3) when $\tilde{A}$ and $\tilde{A}_0$ evolve on the fast length scale $\bar{x}$ (i.e. x_1). For simplicity we consider only the perfectly tuned case where $\bar{\kappa}_i = 0$. The resulting solutions will not match directly onto the linear Tollmien–Schlichting wave solutions as $\bar{x} \to -\infty$ when the linear growth terms are neglected in (8.2) and (8.3). However, as shown in Wundrow *et al.* (1994) and Goldstein (1994), the amplitude equations (8.2) and (8.3) (or the system of critical-layer equations), with the linear growth rate terms omitted and with $\bar{\kappa}_i = 0$, can be solved subject to the upstream boundary conditions (instead of (6.37))

$$\tilde{A}_0 \to a_0, \quad \tilde{A} \to \mathrm{e}^{\mathrm{i}\pi/4}\mathrm{e}^{b\bar{x}} \quad \text{as} \quad \bar{x} \to -\infty, \tag{9.3}$$

where a_0 is a real constant and b is determined from an implicit relationship

$$b = \tfrac{2}{5}a_0 \int_0^\infty \mathrm{e}^{-2\tilde{\lambda}\xi^3/3 - 2b\xi}\xi^2 \mathrm{d}\xi. \tag{9.4}$$

The above equation can be solved numerically by using an iteration method for a given a_0. The amplitudes $\tilde{A}_0$ and $\tilde{A}$ are related to A_0 and A in (4.1) by (6.17) and $\bar{x}$ is related to x_1 in (9.2) by (6.10) and (6.16).

The self-interaction, mutual-interaction and back-reaction terms drop out of (8.2) and (8.3) when $\tilde{A} \ll 1$. Therefore,

$$\frac{\mathrm{d}\tilde{A}}{\mathrm{d}\bar{x}} = \sigma\bar{\kappa}_{ob}\tilde{A} + \tfrac{2}{5}\mathrm{i}\int_{-\infty}^{\bar{x}} K_1 \tilde{A}_0(\tilde{x})\tilde{A}^*(2\tilde{x} - \bar{x})\mathrm{d}\tilde{x}, \tag{9.5}$$

$$\frac{\mathrm{d}\tilde{A}_0}{\mathrm{d}\bar{x}} = \sigma\bar{\kappa}_0\tilde{A}_0, \tag{9.6}$$

where K_1 is given by (8.4) and we have put

$$\sigma\bar{\kappa}_{ob} = \kappa_{ob}/\hat{\kappa}, \quad \sigma\bar{\kappa}_0 = \kappa_0/\hat{\kappa}. \tag{9.7}$$

The plane-wave amplitude $\tilde{A}_0$ is a slowly varying function of $\bar{x}$ and is given by

$$\tilde{A}_0 = a_0\mathrm{e}^{\bar{\kappa}_0\hat{x}}, \tag{9.8}$$

where

$$\hat{x} = \sigma\bar{x}. \tag{9.9}$$

Goldstein (1994) shows that the relevant solution to (9.5) has the standard WKBJ form

$$\tilde{A} = \mathrm{e}^{\mathrm{i}\pi/4}\hat{a}(\hat{x})\exp\left(\frac{1}{\sigma}\int_0^{\hat{x}} \hat{b}(\xi)\mathrm{d}\xi\right). \tag{9.10}$$

Substituting this into (9.5) and equating to zero the coefficients of the first two powers of σ, we obtain

$$\hat{b}(\hat{x}) = \frac{2}{5}\tilde{A}_0(\hat{x})\int_0^\infty \mathrm{e}^{-2\tilde{\lambda}\xi^3/3 - 2\hat{b}(\xi)\xi}\xi^2\mathrm{d}\xi, \tag{9.11}$$

$$\hat{a}(\hat{x}) = C_0\hat{b}^{(\bar{\kappa}_{ob}/\bar{\kappa}_0)}\left(\hat{b}'/\hat{b}\right)^{1/2}, \tag{9.12}$$

where the prime denotes differentiation with respect to $\hat{x}$ and C_0 is a real constant.

It now follows that

$$\tilde{A}_0 \to a_0, \quad \tilde{A} \to \mathrm{e}^{\mathrm{i}\pi/4}\hat{a}(0)\mathrm{e}^{\hat{b}(0)\bar{x}} \quad \text{as} \quad \hat{x} \to 0, \tag{9.13}$$

and therefore that (9.8) and (9.10) match onto the upstream asymptotic behaviour (9.3) of the full non-equilibrium solutions to (8.2) and (8.3) if we put

$$\hat{a}(0) = 1, \quad \hat{b}(0) = b. \tag{9.14}$$

It also follows from (9.8), (9.11) and (9.12) that

$$\tilde{A}_0 \to 0, \quad \hat{b} \to \tilde{A}_0/(5\tilde{\lambda}), \quad \hat{a} \to C_0 \bar{\kappa}_0^{1/2} \left(\frac{a_0}{5\tilde{\lambda}}\right)^{\bar{\kappa}_{ob}/\bar{\kappa}_0} \mathrm{e}^{\bar{\kappa}_{ob}\hat{x}} \quad \text{as} \quad \hat{x} \to -\infty, \tag{9.15}$$

and consequently that

$$\tilde{A} \to C_0 \mathrm{e}^{\mathrm{i}\pi/4} \bar{\kappa}_0^{1/2} \left(\frac{a_0}{5\tilde{\lambda}}\right)^{\bar{\kappa}_{ob}/\bar{\kappa}_0} \exp\left[\bar{\kappa}_{ob}\hat{x} + \frac{a_0}{\sigma 5 \bar{\kappa}_0 \tilde{\lambda}}(\mathrm{e}^{\bar{\kappa}_0 \hat{x}} - 1)\right] \quad \text{as} \quad \hat{x} \to -\infty. \tag{9.16}$$

As shown in Goldstein (1994), this matches onto the downstream behaviour of the solution to the viscous parametric-resonance equation:

$$\frac{\mathrm{d}\tilde{A}}{\mathrm{d}\hat{x}_1} = \bar{\kappa}_{ob}\tilde{A} + \frac{\mathrm{i}}{5\tilde{\lambda}} \hat{A}_0 \tilde{A}^*, \tag{9.17}$$

$$\frac{\mathrm{d}\hat{A}_0}{\mathrm{d}\hat{x}_1} = \bar{\kappa}_0 \hat{A}_0, \tag{9.18}$$

where we have put

$$\hat{x}_1 \equiv \hat{x} - \frac{1}{\bar{\kappa}_0} \ln \sigma, \tag{9.19}$$

$$\hat{A}_0 \equiv \frac{1}{\sigma} \tilde{A}_0. \tag{9.20}$$

The solutions to these equations satisfy the upstream boundary conditions

$$\tilde{A} \to a^{(0)} \mathrm{e}^{\bar{\kappa}_{ob}\hat{x}_1}, \quad \hat{A}_0 \to a_0 \mathrm{e}^{\bar{\kappa}_0 \hat{x}_1} \quad \text{as} \quad \hat{x}_1 \to -\infty, \tag{9.21}$$

and therefore match onto the linear Tollmien–Schlichting wave solutions. In fact these are the equations obtained by Mankbadi *et al.* (1993) for a Blasius boundary layer by introducing the appropriate slow scale directly into the Navier–Stokes equation (see also (8.6) and (8.7)). Wundrow *et al.* (1994) and Goldstein (1994) show that the solution to (9.17) behaves like

$$\tilde{A} \sim \tilde{C}_0 \mathrm{e}^{\mathrm{i}\pi/4} \exp\left(\bar{\kappa}_{ob}\hat{x}_1 + \frac{a_0}{5\bar{\kappa}_0\tilde{\lambda}} \mathrm{e}^{\bar{\kappa}_0 \hat{x}_1}\right) \quad \text{as} \quad \hat{x}_1 \to \infty, \tag{9.22}$$

and will therefore match onto the upstream asymptotic behaviour (9.16) of the solution to (9.5) if we put

$$\tilde{C}_0 = C_0 \bar{\kappa}_0^{1/2} \left(\frac{\sigma a_0}{5\tilde{\lambda}}\right)^{\bar{\kappa}_{ob}/\bar{\kappa}_0} \exp\left(-\frac{a_0}{\sigma 5 \bar{\kappa}_0 \tilde{\lambda}}\right). \tag{9.23}$$

The approximation (9.17) becomes invalid when $\bar{\kappa}_0 \hat{x}_1 = O(\ln \sigma)$ because the non-equilibrium effects become of the same order as the viscous effects and the flow begins to evolve on the faster scale x_1. This shows that the Tollmien–Schlichting waves will ultimately evolve into the full non-equilibrium solution to (8.2) and (8.3) if the initial amplitude of the oblique modes is sufficiently (exponentially) small at the start of parametric resonance. The fully coupled stage is then of the non-equilibrium type considered by G&L rather than the quasi-equilibrium type of Mankbadi *et al.* (1993), even in a Blasius boundary layer.

10. Discussion and results

We have obtained the generalized scaling (3.2)–(3.11) for the fully coupled resonant-triad interactions in zero- or non-zero-pressure-gradient boundary layers. Table 1 shows that the scalings of previously studied boundary layers can be recovered by suitable choice of the parameters r, m, λ and $\bar{\mu}$.

The non-equilibrium critical-layer dynamics, corresponding $m = r$, are determined by the system of critical-layer equations (6.19) and (6.22)–(6.24) and the jump conditions (6.33) and (6.34) with the transverse boundary conditions (6.28) and upstream boundary condition (6.37) or (9.3). The variables have been normalized to eliminate the basic mean-flow-dependent parameters everywhere except in the linear growth rate terms, that appear in the jump conditions (6.33) and (6.34). The nonlinear equations (6.19) and (6.22)–(6.24) do not include any basic-flow-dependent parameters explicitly as explained in §6. The generalized non-equilibrium critical-layer analysis presented in §§4–8 is obtained with the scaling (3.2)–(3.4) and (3.12)–(3.14) when $1 \leqslant r \leqslant 3$. The finite–viscosity version of G&L's adverse-pressure-gradient boundary layer analysis is obtained by taking $r = 3$ and the scalings and amplitude equations for the final fully coupled stage of Wundrow *et al.* (1994) is recovered by putting $r = 3/2$ and $\bar{\mu} = \lambda = 0$. It is also shown in the previous section that the final non-equilibrium stage for the Blasius boundary layer, which was first studied by Goldstein (1994), corresponds to the case when $r = 2$ and $\bar{\mu} = 0$.

The inviscid analysis of G&L can be extended to obtain the amplitude equations for finite viscosity as was done by Wu *et al.* (1993) and Wu (1995). The amplitudes of the instability waves $\tilde{A}$ and $\tilde{A}_0$ are still governed by the integro-differential equations (8.2) and (8.3) which are the same as the inviscid ones in G&L, but with viscous effects now appearing in the kernel functions and the scaling factor σ^{3-r} appearing in the linear growth rates.

We can recover the scalings and amplitude equations for the Blasius and favourable-pressure-gradient boundary layers, where the critical layers are of quasi-equilibrium type and which were studied by Mankbadi *et al.* (1993) and Wu (1993), by taking the viscous limit of the non-equilibrium amplitude equations and by rescaling the non-equilibrium solution by (8.8) and (8.9). It is assumed that the mutual-interaction and back-reaction terms in the plane-wave amplitude equation become negligibly small in the viscous limit but this can also be verified from the analytical solution of Wu (1995).

Since Wu's (1995) result shows that the final formula for the kernel function K_5 in (8.3) is very complex, we decided to solve numerically the critical-layer equations with jump conditions in the fully coupled case. The amplitude equations are easier to solve when the mutual-interaction and back-reaction terms can be neglected in the amplitude equation for the two-dimensional mode.

Results of the numerical computations will be presented in the following subsections. The system of critical-layer equations is solved by using the numerical method described in §7. The amplitude equations (8.2) and (8.3) (with the mutual-interaction and back-reaction terms omitted in (8.3)) are solved by using numerical method similar to the one used in G&L. The viscous-limit equations (8.6) and (8.7) are solved with a predictor-corrector method explained in §7.

10.1. *Numerical results for the $O(1)$ linear-growth-rate case*

We first present the computational results for the case where the linear growth terms in the jump conditions (6.33) and (6.34) and, consequently, in the amplitude equations (8.2) and (8.3) are $O(1)$. The upstream boundary condition is given by (6.37). In this

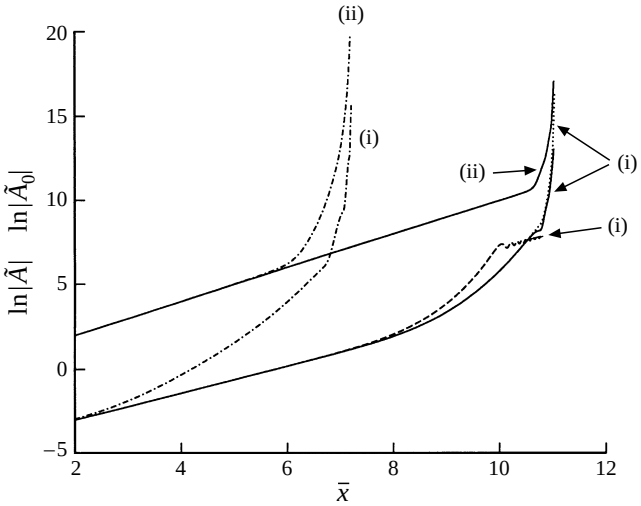

FIGURE 2. $\ln|\tilde{A}|$ and $\ln|\tilde{A}_0|$, curves (i) and (ii) respectively, *vs.* $\bar{x}$ for $\tilde{\lambda} = 10^3$, $|a^{(0)}| = 0.01$, $\arg(a^{(0)}) = 0$ and $\bar{\kappa}_i = 0$ (solid curve, finite-viscosity solution; dotted, finite-viscosity solution with linear two-dimensional mode; dashed, viscous limit solution; dot-dashed, inviscid solution).

case, it is convenient to study the effect of the viscosity by choosing

$$\hat{\kappa} = \kappa_0, \tag{10.1}$$

so that

$$\kappa_{ob}/\hat{\kappa} = 4/5, \quad \kappa_0/\hat{\kappa} = 1, \tag{10.2}$$

from (6.41). The system of equations (6.19), (6.22)–(6.24), (6.33) and (6.34) with (6.28) and (6.37), or the equivalent amplitude equations (8.2) and (8.3) with (6.37), contain four controllable parameters: $\tilde{\lambda}$, which accounts for the viscous effect; $|a^{(0)}|$, which accounts for the initial magnitude of the oblique-mode amplitude; $\arg(a^{(0)})$, which accounts for the initial phase of the oblique-mode amplitude; and $\bar{\kappa}_i$, which accounts for the effect of the initial wavenumber detuning. The normalized initial amplitude of the plane wave is one as in (6.37). The effect of each of these parameters is discussed below.

Figure 2 shows the numerical results for $\tilde{\lambda} = 10^3$, $|a^{(0)}| = 0.01$, $\arg(a^{(0)}) = 0$ and $\bar{\kappa}_i = 0$. The solutions of the inviscid amplitude equations ($\tilde{\lambda} = 0$) with the same initial conditions are plotted as the dot-dashed curve. The scaled amplitudes initially exhibit linear growth. The plane-wave amplitude continues to grow linearly and it reaches a level that produces a parametric-resonance growth in the oblique modes, which then allows them to grow until they become large enough to interact with themselves (self-interaction). The scaled amplitudes of both the oblique and plane waves then exhibit a rapid increase in growth and ultimately end in a singularity. The viscosity does not alter the general behaviour of the solution, but it delays the onset of the parametric-resonance and self-interaction and also the appearance of the singularity.

The solution of the oblique-mode amplitude equation (8.2) for the same initial conditions, but with the plane wave $\tilde{A}_0$ constrained to grow linearly (i.e. $\tilde{A}_0 = e^{\bar{x}}$), is also plotted in figure 2 as the dotted curve (a straight dotted line for the plane-wave amplitude is not plotted). Comparing the solid curve with the dotted one for the oblique mode, we can note that the oblique-mode growth rate of the solid curve (with full plane-wave equation) is slightly decreased at the start of the fully coupled

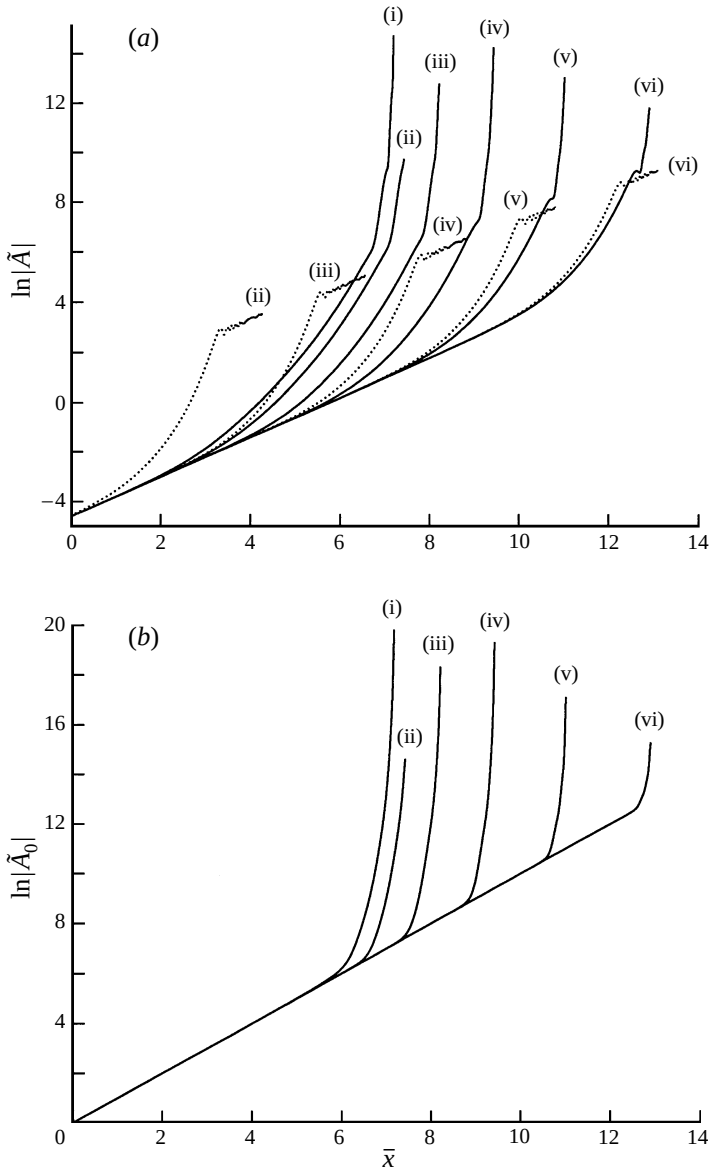

FIGURE 3. (*a*) $\ln|\tilde{A}|$ *vs.* $\bar{x}$ and (*b*) $\ln|\tilde{A}_0|$ *vs.* $\bar{x}$: $|a^{(0)}| = 0.01$, $\arg(a^{(0)}) = 0$, $\bar{\kappa}_i = 0$ and $\tilde{\lambda} = 0, 1, 10, 10^2, 10^3, 10^4$, curves (i)–(vi) respectively (solid, finite-viscosity solution; dotted, viscous-limit solution).

interaction stage where $\bar{x}$ is about 10.7. This is due to the mutual-interaction and back-reaction terms in the plane-wave amplitude equation or the integral term, which represents the nonlinear jump across the critical layer, on the right-hand side of (6.34).

The dashed curve in figure 2 is obtained by solving the viscous-limit equations (8.6) and (8.7). The plane-wave amplitude grows linearly although we do not show a dashed line for that. The parametric resonance growth rate of the oblique mode obtained from the non-equilibrium equations is smaller than that predicted by the viscous-limit equations.

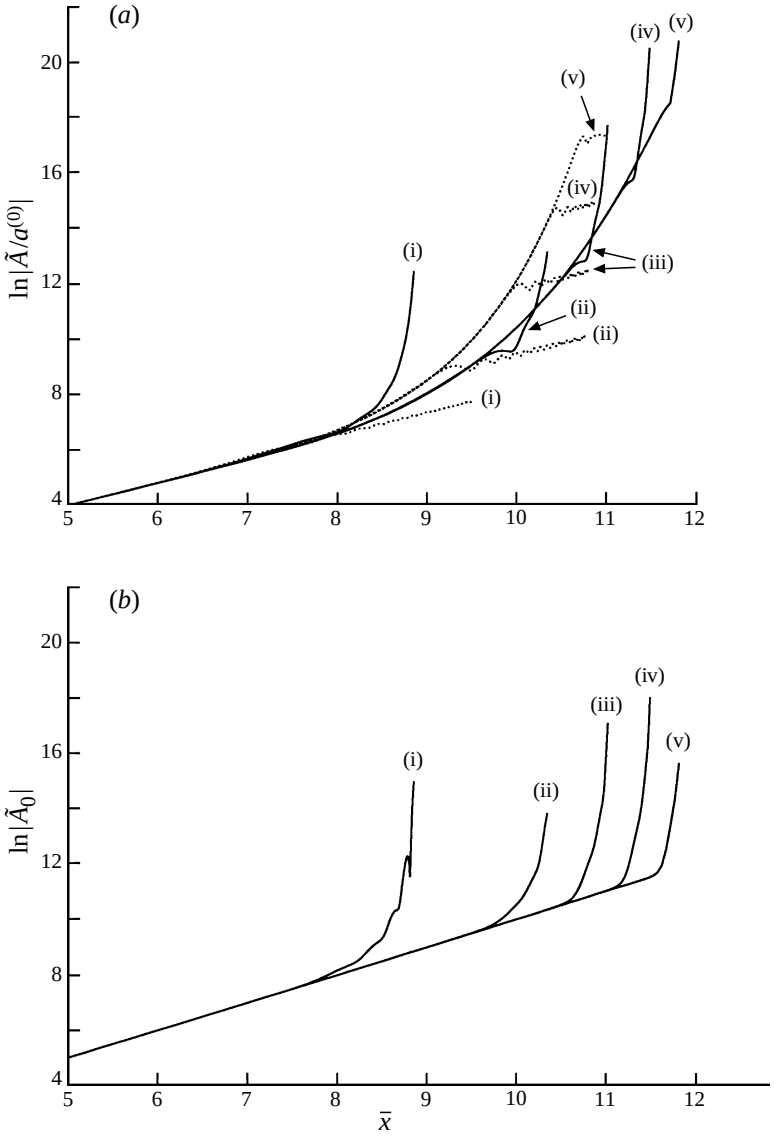

FIGURE 4. (*a*) $\ln|\tilde{A}/a^{(0)}|$ *vs.* $\bar{x}$ and (*b*) $\ln|\tilde{A}_0|$ *vs.* $\bar{x}$, for $\tilde{\lambda} = 10^3$, $\arg(a^{(0)}) = 0$, $\bar{\kappa}_i = 0$ and $|a^{(0)}| = 1, 10^{-1}, 10^{-2}, 10^{-3}, 10^{-4}$, curves (i)–(v) respectively (solid, finite-viscosity solution; dotted, viscous-limit solution).

Figure 3 illustrates the effect of the viscosity. The viscous parameter $\tilde{\lambda}$ is varied from 0 (inviscid) to 10^4 while $|a^{(0)}| = 0.01$, $\arg(a^{(0)}) = 0$ and $\bar{\kappa}_i = 0$ remain unchanged. The corresponding solutions of the viscous-limit equations are plotted as dotted curves (a straight dotted line is not plotted in figure 3*b*). The difference between the non-equilibrium critical-layer solution and the quasi-equilibrium critical-layer solution becomes smaller, at least in the parametric-resonance region, as $\tilde{\lambda}$ becomes larger. The parametric-resonance growth rates of the viscous-limit solutions are always larger than those of the corresponding finite viscous non-equilibrium solutions. Curves (vi) corresponding to $\tilde{\lambda} = 10^4$ show that the non-equilibrium solution of the oblique mode

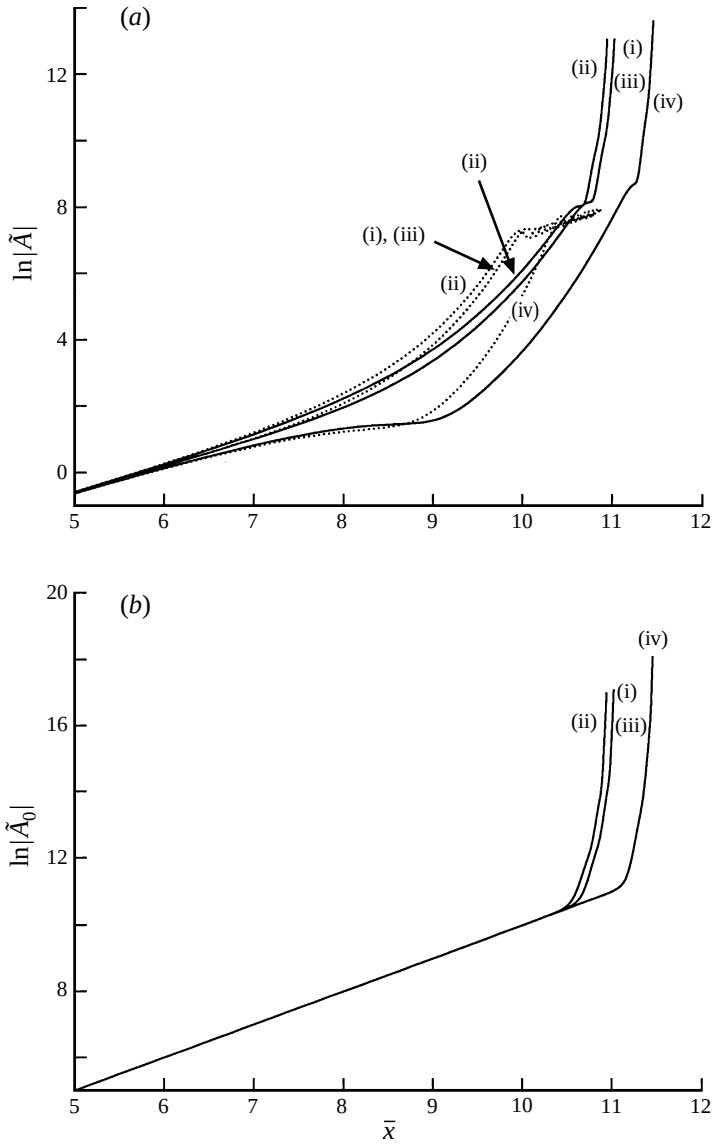

FIGURE 5. (*a*) $\ln|\tilde{A}|$ *vs.* $\bar{x}$ and (*b*) $\ln|\tilde{A}_0|$ *vs.* $\bar{x}$, for $\tilde{\lambda} = 10^3$, $|a^{(0)}| = 0.01$, $\bar{\kappa}_i = 0$ and $\arg(a^{(0)}) = 0, \pi/4, \pi/2, 13\pi/18$, curves (i)–(iv) respectively (solid, finite-viscosity solution; dotted, viscous-limit solution).

qualitatively agrees with the corresponding viscous-limit solution until the end of the first oscillation or until $\bar{x}$ is about 12.7 for the solid curve. However, the scaled amplitudes of both the oblique and plane waves always end in a singularity at a finite downstream position even though the viscous parameter is very large.

These numerical results are consistent with the results of Goldstein (1994) and Wu *et al.* (1997), who show that the final critical layer becomes of non-equilibrium type although the critical layer in the earlier stage is of quasi-equilibrium type. However, both analyses did not start with the same initial amplitudes of the resonant triad as those in Mankbadi *et al.* (1993). The initial amplitude of the oblique mode was

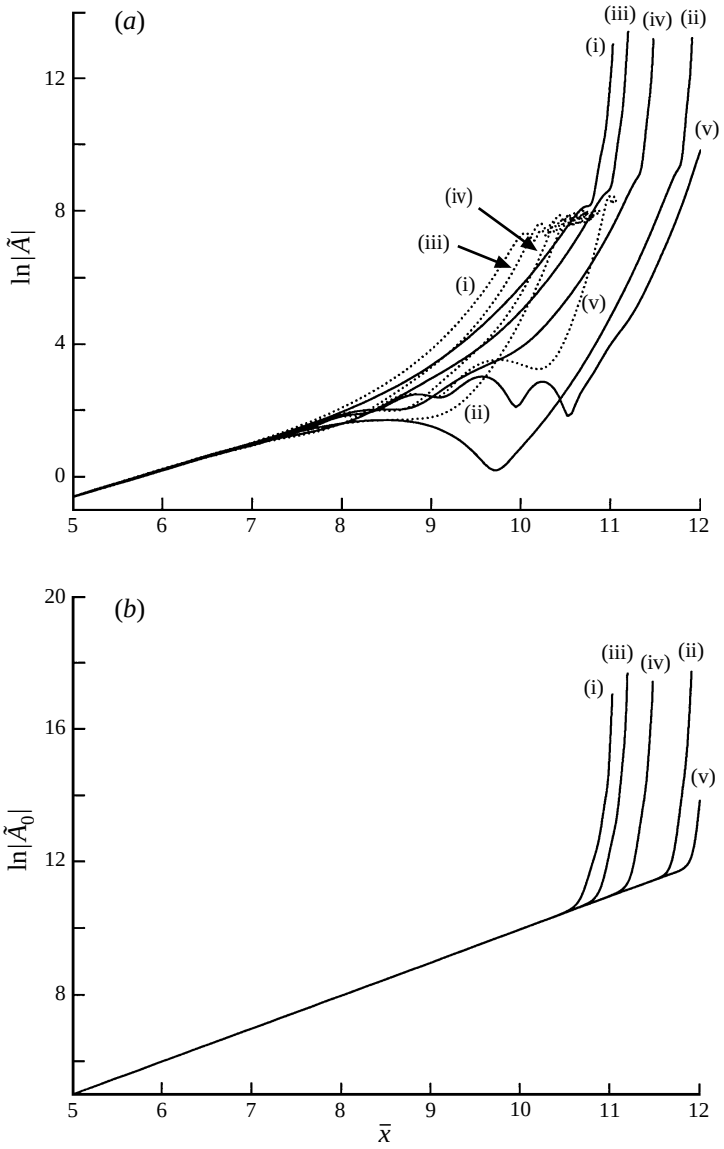

FIGURE 6. (*a*) $\ln|\tilde{A}|$ *vs.* $\bar{x}$ and (*b*) $\ln|\tilde{A}_0|$ *vs.* $\bar{x}$, for $\tilde{\lambda} = 10^3$, $|a^{(0)}| = 0.01$, $\arg(a^{(0)}) = 0$ and $\bar{\kappa}_i = 0, 1, 2, 4, 8$, curves (i)–(v) respectively (solid, finite-viscosity solution; dotted, viscous-limit solution).

sufficiently smaller in the former case and that of the plane wave was negligibly smaller in the latter case. The present computational results with large values of $\tilde{\lambda}$, shown in figure 3, indicate that the later stage of the evolution of the viscous resonant triad considered by Mankbadi *et al.* (1993) (we can also add a small non-zero pressure gradient as discussed in §3 and §8) will also be governed by the non-equilibrium critical-layer dynamics. The solutions of the quasi-equilibrium amplitude equations of Mankbadi *et al.* (1993) correspond to the dotted curves in figure 3 (except the modified linear growth rates).

Figure 4 shows the effect of varying the normalized initial oblique-mode amplitude $|a^{(0)}|$. The viscous parameter $\tilde{\lambda} = 10^3$, and $\arg(a^{(0)})$ and $\bar{\kappa}_i$ are set equal to zero. The

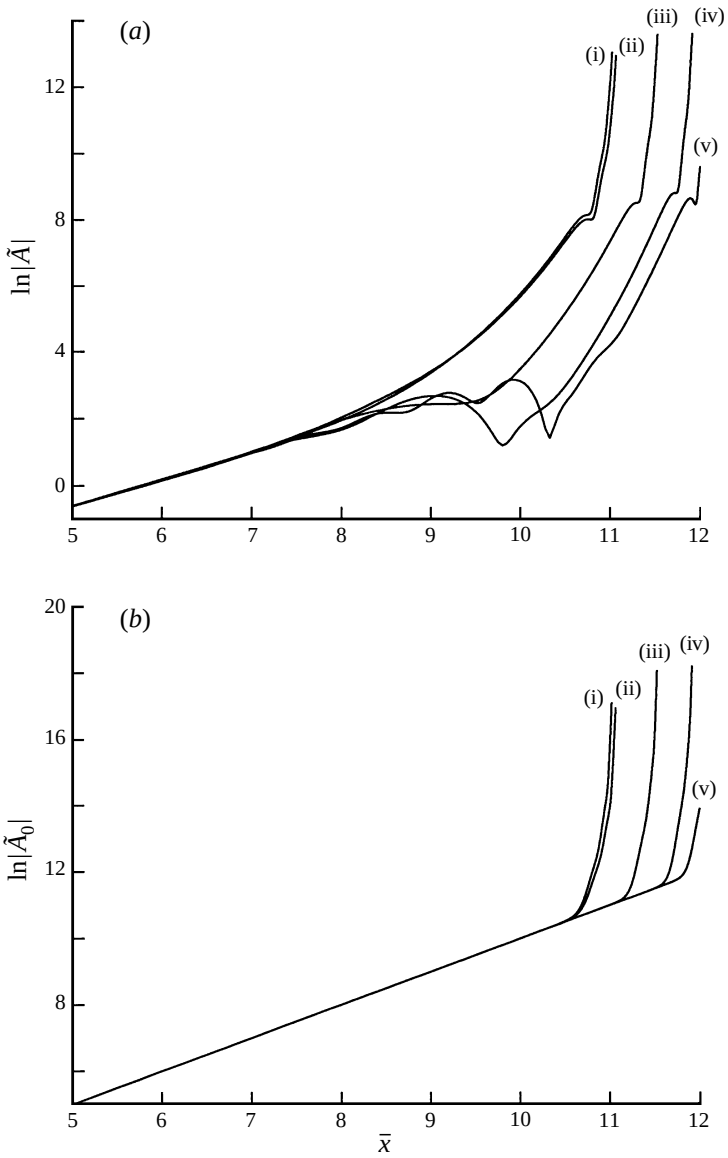

FIGURE 7. (*a*) $\ln|\tilde{A}|$ *vs.* $\bar{x}$, and (*b*) $\ln|\tilde{A}_0|$ *vs.* $\bar{x}$, for $\tilde{\lambda} = 10^3$, $|a^{(0)}| = 0.01$, $\arg(a^{(0)}) = 0$ and $\bar{\kappa}_i = 0, -1, -2, -4, -8$, curves (i)–(v) respectively.

net effect of reducing $|a^{(0)}|$ is to delay both the onset of the fully coupled interaction and the ultimate downstream location of the singularity.

Figure 5 shows the effect of varying $\arg(a^{(0)})$, the argument of $a^{(0)}$. Here we put $\tilde{\lambda} = 10^3$, $|a^{(0)}| = 0.01$ and $\bar{\kappa}_i = 0$. The results for $\arg(a^{(0)}) = 0$ are almost identical to the $\arg(a^{(0)}) = \frac{1}{2}\pi$ rad results. As in the inviscid calculations of G&L, the onset of the fully coupled interaction and the position of the singularity occur at the earliest downstream location when $\arg(a^{(0)}) = \frac{1}{4}\pi$ rad.

Figures 6 and 7 illustrate the effect of initial wavenumber detuning. We have fixed $\tilde{\lambda} = 10^3$, $|a^{(0)}| = 0.01$ and $\arg(a^{(0)}) = 0$. The results are similar to the inviscid results of G&L in that increasing the initial wavenumber detuning delays the growth in the

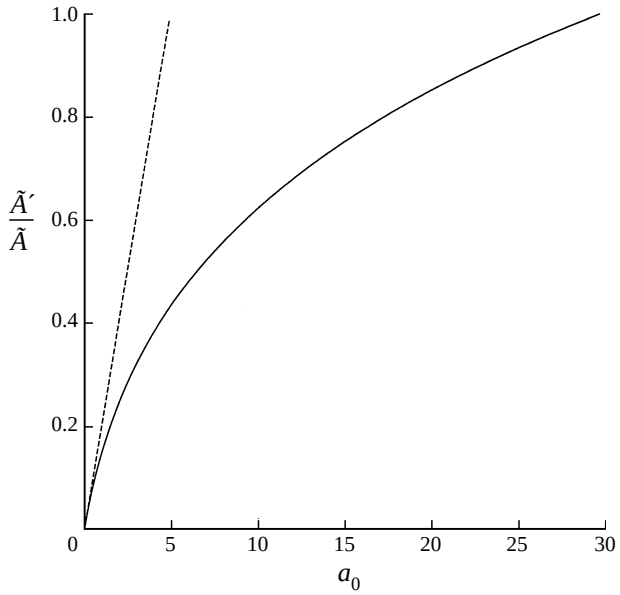

FIGURE 8. $\tilde{A}'/\tilde{A}$ *vs.* a_0 in the parametric-resonance region (solid, non-equilibrium solution; dashed, quasi-equilibrium solution).

oblique-mode amplitude and moves both the onset of the fully coupled stage and the singularity position further downstream. The oblique-mode amplitudes grow almost linearly, but exhibit oscillations, in the parametric-resonance stage when $\bar{\kappa}_i$ is large.

10.2. *Numerical results for the negligibly small linear-growth-rate case*

In a Blasius boundary layer (Goldstein 1994), an initial parametric-resonance growth of quasi-equilibrium type is often followed by a non-equilibrium-type interaction before the self-interaction effects become important. It was shown in §9 (Wundrow *et al.* 1994; Goldstein 1994) that the linear growth terms are negligibly small in the fully coupled non-equilibrium region and that the upstream condition (9.3) should be used instead of (6.37).

Putting

$$\hat{\kappa} = \bar{\lambda}^{1/3}, \tag{10.3}$$

leads to

$$\tilde{\lambda} = 1, \tag{10.4}$$

from (6.16), which means that the viscous parameter can be scaled out of the final equations. The system of equations (6.19), (6.22)–(6.24), (6.33) and (6.34) with (6.28) and (9.3), or the equivalent amplitude equations (8.2) and (8.3) with (9.3), when the linear growth terms are omitted and $\bar{\kappa}_i = 0$, now contain only one controllable parameter, a_0.

Figure 8 shows the oblique-mode growth rate, $\tilde{A}_{\bar{x}}/\tilde{A}$ (or b which is given by (9.4)), in the parametric-resonance region as function of the nearly constant plane-wave amplitude, a_0. The solution of (9.5) without the linear growth term and with $\tilde{A}_0 = a_0$ is plotted as a solid curve. The dashed curve represents the viscous-limit solution, $\tilde{A}_{\bar{x}}/\tilde{A} = \frac{1}{5}a_0$, which is obtained from (8.6) with the linear-growth and self-interaction terms omitted. This figure shows that the oblique-mode growth rates obtained from the

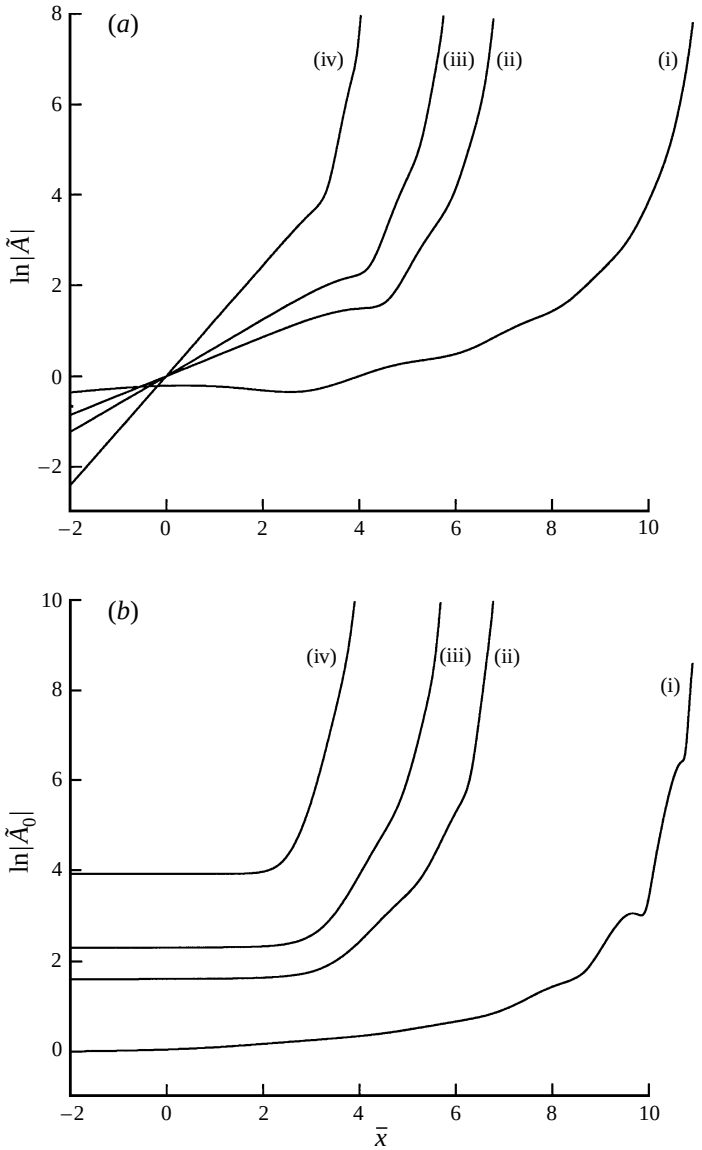

FIGURE 9. (*a*) $\ln|\tilde{A}|$ *vs.* $\bar{x}$ and (*b*) $\ln|\tilde{A}_0|$ *vs.* $\bar{x}$, for $a_0 = 1, 5, 10, 50$, curves (i)–(iv) respectively.

non-equilibrium equation with finite viscosity are always lower than those predicted by the quasi-equilibrium critical-layer equations in the parametric-resonance regime. This is consistent with the result obtained for the $O(1)$ linear-growth-rate case as given in figures 2 and 3. Khokhlov (1993) showed that the solutions of the non-equilibrium critical-layer equations are in reasonably good agreement with the experimental results of Kachanov, Kozlov & Levchenko (1977) and Kachanov & Levchenko (1984) in the parametric-resonance stage.

Figure 9 illustrates the effect of varying a_0. In the non-equilibrium parametric resonance region the plane-wave amplitude $\tilde{A}_0$ remains constant but the oblique-mode amplitude $\tilde{A}$ continues to exhibit parametric-resonance growth until these modes become large enough to interact with themselves. This self-interaction produces a

further enhancement in their growth, which ends in a singularity at a finite downstream position. This explosive growth is then transferred to the plane wave through the mutual-interaction and back-reaction terms. The oblique-mode growth rate in the parametric-resonance stage increases with a_0. The plane-wave and oblique-mode amplitudes both become singular at a finite downstream position as in the $O(1)$ linear-growth-rate case.

The author would like to thank Dr Lennart S. Hultgren for suggesting him solving the partial differential critical-layer equations directly by using numerical methods and Drs M. E. Goldstein, David W. Wundrow, S. J. Leib, Lennart S. Hultgren and R. R. Mankbadi for many helpful discussions. Drs S. J. Cowley and X. Wu are also thanked for their useful comments.

Appendix A. Coefficients J_1, J_2, J_3, J_4 and J_5 in (4.17)

$$J_1 = \int_0^\infty \left[U^2 - \frac{1}{U^2} + \frac{1}{\tau_w^2 y^2} - \sigma^{r-1}\frac{\bar{\mu}}{\tau_w^3 y(y+1)}\right] \mathrm{d}y, \tag{A 1}$$

$$J_2 = \int_0^\infty \left[-\frac{1}{U^3} + \frac{2}{U^2} - U + \frac{1}{\tau_w^3 y^3} - \frac{2}{\tau_w^2 y^2} - \sigma^{r-1}\frac{3\bar{\mu}}{2\tau_w^4 y^2} + \ldots\right] \mathrm{d}y, \tag{A 2}$$

$$J_3 = \int_0^\infty \left[1 - \frac{3}{U^4} + \frac{8}{U^3} - \frac{6}{U^2} + \frac{3}{\tau_w^4 y^4} - \frac{8}{\tau_w^3 y^3} + \frac{6}{\tau_w^2 y^2} + \frac{\tau_0^2}{4\tau_w^5 y(y+1)} - \sigma^{r-1}\frac{6\bar{\mu}}{\tau_w^5 y^3} + \ldots\right] \mathrm{d}y, \tag{A 3}$$

$$J_4 = \int_0^\infty U^2 \int_y^\infty \left(U^2 - \frac{1}{U^2}\right) \mathrm{d}\hat{y}\mathrm{d}y, \tag{A 4}$$

$$J_5 = \lim_{y,\hat{c}\to 0}\left(\frac{\partial \Omega_1}{\partial \hat{c}} + \frac{\bar{\gamma}}{\bar{c}}\Omega_2\right). \tag{A 5}$$

Appendix B. Normalization and the critical-layer equation

The dependent variables in (6.19), (6.21) and (6.22) are normalized as

$$\tilde{Q}^{(1)} = (Y_c M)^{1/2}/(\hat{\kappa}^2 \bar{c}\sin\theta) Q^{(1)} \mathrm{e}^{\mathrm{i}X_0/2}, \tag{B 1}$$

$$\left\{\tilde{Q}^{(l)}_{n,m}, \tilde{Q}^{(4L)}_{2,0}, \tilde{W}^{(l)}_{n,m}\right\} = \left\{\hat{Q}^{(l)}_{n,m}, \hat{Q}^{(4L)}_{2,0}, \hat{W}^{(l)}_{n,m}\right\} \mathrm{e}^{\mathrm{i}nX_0/2}, \tag{B 2}$$

where

$$\hat{Q}^{(2)}_{1,1} = (2\pi\bar{\alpha})^{1/2} M\cos\theta/(\hat{\kappa}^2 \tau_w^{1/2}\bar{c}^{1/2}\tan\theta) Q^{(2)}_{1,1}, \tag{B 3}$$

$$\left\{\hat{Q}^{(2)}_{0,0}, \hat{Q}^{(2)}_{0,2}, \hat{Q}^{(2)}_{2,0}, \hat{W}^{(2)}_{0,2}, \hat{W}^{(2)}_{2,2}\right\} = \frac{M}{\hat{\kappa}^2\tan^2\theta}\left\{Q^{(2)}_{0,0}, Q^{(2)}_{0,2}, Q^{(2)}_{2,0}, \frac{\tan\theta}{\hat{\kappa}}W^{(2)}_{0,2}, \frac{\tan\theta}{\hat{\kappa}}W^{(2)}_{2,2}\right\}, \tag{B 4}$$

$$\left\{\hat{Q}^{(3)}_{1,1}, \hat{Q}^{(3)}_{3,1}, \hat{W}^{(3)}_{1,1}, \hat{W}^{(3)}_{3,1}\right\} = \frac{\bar{c}M^{3/2}\cos\theta}{\hat{\kappa}^3 Y_c^{1/2}\tan^2\theta}\left\{Q^{(3)}_{1,1}, Q^{(3)}_{3,1}, \frac{\tan\theta}{\hat{\kappa}}\left(W^{(3)}_{1,1} - W^{(3a)}_{1,1}\right), \frac{\tan\theta}{\hat{\kappa}}W^{(3)}_{3,1}\right\}, \tag{B 5}$$

$$\left\{\hat{Q}^{(4)}_{2,0}, \hat{Q}^{(4L)}_{2,0}\right\} = 2\pi\bar{\alpha}M/(\hat{\kappa}^4\tau_w^3\bar{c})\left\{Q^{(4)}_{2,0} - Q^{(4a)}_{2,0} - Q^{(4L)}_{2,0}, Q^{(4L)}_{2,0}\right\}, \tag{B 6}$$

$W^{(3a)}_{1,1}$ and $Q^{(4a)}_{2,0}$ are the terms which do not play any active role in calculating the velocity jump across the critical layer, and $Q^{(4L)}_{2,0}$ is the term which produces the linear velocity jump across the critical layer for the two-dimensional mode.

The critical-layer equations (6.22) are obtained by substituting (B 1)–(B 6) along with (6.15) into equations (5.37)–(5.40) and Appendix B of G&L. For notational simplicity, we have omitted the tilde on $\tilde{\eta}$, $\tilde{A}$, $\tilde{A}_0$, $\tilde{Q}^{(1)}$, $\tilde{Q}^{(l)}_{n,m}$, $\tilde{U}^{(l)}_{n,m}$, $\tilde{V}^{(l)}_{n,m}$, $\tilde{W}^{(l)}_{n,m}$, and $\tilde{q}^{(3)}_{n,1}$ in the following equations of this Appendix. The expressions for the terms on the right-hand sides of (6.22) are

$$G^{(2)}_{0,0} = AQ^{(1)^*}_{\eta\eta}, \tag{B 7}$$

$$G^{(2)}_{0,2} = 2\mathrm{i}W^{(2)}_{0,2} + \mathrm{Re}\left(AQ^{(1)^*}_{\eta\eta}\right), \tag{B 8}$$

$$H^{(2)}_{0,2} = \mathrm{i}\left[2\tau(\sin^2\theta)|Q^{(1)}|^2 + \mathrm{Im}\left(AQ^{(1)^*}_{\eta}\right)\right], \tag{B 9}$$

$$G^{(2)}_{2,0} = 2\mathrm{i}\tau(\sin^2\theta)\left(Q^{(1)^2}\right)_\eta - AQ^{(1)}_{\eta\eta}, \tag{B 10}$$

$$H^{(2)}_{2,2} = \tfrac{1}{2}AQ^{(1)}_{\eta}, \tag{B 11}$$

$$R^{(3)}_{1,1} = 2\cos^2\theta A_0 Q^{(1)^*}_{\eta\eta} + \tfrac{1}{2}\mathrm{i}\left[A\left(2\mathrm{Re}Q^{(2)}_{0,0} + Q^{(2)}_{0,2} + W^{(2)}_{0,2\eta}\right) - A^*Q^{(2)}_{2,0}\right]_\eta + \tau\sin^2\theta\left(2Q^{(1)}U^{(2)}_{0,2} - Q^{(1)}_{\eta}V^{(2)}_{0,2} + Q^{(1)^*}_{\eta}V^{(2)}_{2,0}\right)_\eta, \tag{B 12}$$

$$H^{(3)}_{1,1} = \cos^2\theta A_0 Q^{(1)^*}_{\eta} + \tfrac{1}{2}\mathrm{i}\left(AW^{(2)}_{0,2} - A^*W^{(2)}_{2,2}\right)_\eta - \tfrac{1}{2}\tau\sin^2\theta\left[Q^{(1)}\left(2\mathrm{Re}U^{(2)}_{0,0} - U^{(2)}_{0,2} - W^{(2)}_{0,2}\right) + Q^{(1)}_{\eta}V^{(2)}_{0,2} - Q^{(1)^*}U^{(2)}_{2,0} - Q^{(1)^*}_{\eta}V^{(2)}_{2,0}\right], \tag{B 13}$$

$$R^{(3)}_{3,1} = -\tfrac{2}{3}\cos^2\theta A_0 Q^{(1)}_{\eta\eta} + \mathrm{i}A\left(\tfrac{1}{2}Q^{(2)}_{2,0} - \tfrac{1}{3}W^{(2)}_{2,2\eta}\right)_\eta + \tfrac{1}{3}\tau\sin^2\theta\left[4Q^{(1)}\left(U^{(2)}_{2,0} - 2W^{(2)}_{2,2}\right) - Q^{(1)}_{\eta}V^{(2)}_{2,0}\right]_\eta, \tag{B 14}$$

$$H^{(3)}_{3,1} = \cos^2\theta A_0 Q^{(1)}_{\eta} + \tfrac{1}{2}\mathrm{i}AW^{(2)}_{2,2\eta} - \tfrac{1}{2}\tau\sin^2\theta\left(Q^{(1)}U^{(2)}_{2,0} - Q^{(1)}_{\eta}V^{(2)}_{2,0} - 2Q^{(1)}W^{(2)}_{2,2}\right), \tag{B 15}$$

$$G^{(4)}_{2,0} = 2\mathrm{i}A_0\mathrm{Re}Q^{(2)}_{0,0\eta} + \mathrm{i}\tau\tan^2\theta\left[\left(V^{(2)}_{2,0}\mathrm{Re}U^{(2)}_{0,0} - V^{(2)}_{0,2}W^{(2)}_{2,2}\right)_\eta - 4\left(U^{(2)}_{2,0}\mathrm{Re}U^{(2)}_{0,0} - U^{(2)}_{0,2}W^{(2)}_{2,2}\right)\right]_\eta + \mathrm{i}\sec^2\theta A\left(q^{(3)}_{1,1} - W^{(3)}_{1,1\eta}\right)_\eta - \tau\tan^2\theta\left[\left(Q^{(1)}V^{(3)}_{1,1}\right)_\eta + 4Q^{(1)}\left(W^{(3)}_{1,1} - V^{(3)}_{1,1\eta}\right)\right]_\eta - \mathrm{i}\sec^2\theta A^*\left(q^{(3)}_{3,1} - \tfrac{1}{3}W^{(3)}_{3,1\eta}\right)_\eta + \tau\tan^2\theta\left[\left(Q^{(1)^*}V^{(3)}_{3,1}\right)_\eta + \tfrac{4}{3}Q^{(1)^*}\left(W^{(3)}_{3,1} - V^{(3)}_{3,1\eta}\right)\right]_\eta, \tag{B 16}$$

where the asterisks denote the complex conjugates, Im denotes the imaginary part, and

$$\tau \equiv \bar{c}/(\tau_w Y_c) \tag{B 17}$$

becomes unity when (4.19) is used.

Appendix C. The Kernel function K_2 in (8.2)

$$
\begin{aligned}
K_2 = & -E(t_1;t_2)\left\{(2t_1+t_2)t_1^2+2\sin^2\theta\int_0^{t_2}E(t_3;t_1)t_1(t_1+2t_2-2t_3)dt_3\right\}\\
& +2(\sin^2\theta)E(t_1;t_2)\int_0^{t_1}\left\{\left[E(t_3;t_1)/E(t_3;0)+E_0(t_1,t_2,t_3|0)\right](t_1-t_3)(t_1+2t_2+3t_3)\right.\\
& -2\left[E^{3/8}(t_2;\tfrac{4}{3}t_1)E^{1/4}(t_2+2t_3;2t_1+t_2)\right]\left[1+2\tilde{\lambda}(t_1-t_3)(t_1+t_2+t_3)^2\right]\\
& \times\left[t_2t_3+4\sin^2\theta\int_0^{t_3}E^{-1}(t_4;t_2)(t_3-t_4)\mathrm{d}t_4\right]\\
& \left.-4\sin^2\theta\left[I(t_1,t_2,t_3|t_2)+I(t_1,t_2,t_3|0)\right]\right\}\mathrm{d}t_3, \qquad \text{(C 1)}
\end{aligned}
$$

where

$$t_1\equiv\bar{x}-x_1,\quad t_2\equiv x_1-x_2, \qquad \text{(C 2)}$$

$$E(t_m;t_n)\equiv\mathrm{e}^{-\tilde{\lambda}(2t_m/3+t_n)t_m^2}, \qquad \text{(C 3)}$$

$$E_0(t_1,t_2,t_3|\hat{t})\equiv\mathrm{e}^{-\tilde{\lambda}\left[(t_1+t_2-\hat{t})(t_2+t_3-\hat{t})^2-(t_2-\hat{t})^3/3\right]}, \qquad \text{(C 4)}$$

$$
\begin{aligned}
I(t_1,t_2,t_3|\hat{t})\equiv & \int_0^{t_3+\hat{t}}E_0(t_1,t_2,t_3|\hat{t})E(t_4;t_1+t_2-\hat{t})\\
& \times(t_4-t_3-\hat{t})\left[1+2\tilde{\lambda}(t_1-t_3)(t_2+t_3-\hat{t})^2\right]\mathrm{d}t_4. \qquad \text{(C 5)}
\end{aligned}
$$

REFERENCES

Anderson, D. A., Tannehill, J. C. & Pletcher, R. H. 1984 *Computational Fluid Mechanics and Heat Transfer*. Hemisphere.

Benney, D. J. & Bergeron, R. F. 1969 A new class of nonlinear waves in parallel flows. *Stud. Appl. Maths* **48**, 181–204.

Cowley, S. J. & Wu, X. 1994 Asymptotic approaches to transition modelling. In *Progress in Transition Modelling, AGARD Rep.* 793, Chap. 3, pp. 1–38.

Craik, A. D. D. 1971 Non-linear resonant instability in boundary layers. *J. Fluid Mech.* **50**, 393–413.

Gear, C. W. 1971 *Numerical Initial Value Problems in Ordinary Differential Equations*. Prentice-Hall.

Goldstein, M. E. 1994 Nonlinear interactions between oblique instability waves on nearly parallel shear flows. *Phys. Fluids* **6**, 724–735.

Goldstein, M. E. 1995 The role of nonlinear critical layers in boundary layer transition. *Phil. Trans. R. Soc. Lond.* A **352**, 425–442.

Goldstein, M. E. & Choi, S. W. 1989 Nonlinear evolution of interacting oblique waves on two–dimensional shear layers. *J. Fluid Mech.* **207**, 97-120. Also Corrigendum, *J. Fluid Mech.* **216**, 659–663.

Goldstein, M. E. & Durbin, P. A. 1986 Nonlinear critical layers eliminate the upper branch of spatially growing Tollmien-Schlichting waves. *Phys. Fluids* **29**, 2344.

Goldstein, M. E., Durbin, P. A. & Leib, S. J. 1987 Roll-up of vorticity in adverse-pressure-gradient boundary layers. *J. Fluid Mech.* **183**, 325–342.

Goldstein, M. E. & Lee, S. S. 1992 Fully coupled resonant-triad interaction in an adverse-pressure-gradient boundary layer. *J. Fluid Mech.* **245**, 523–551 referred to herein as G&L.

Goldstein, M. E. & Lee, S. S. 1993 Oblique instability waves in nearly parallel shear flows. In *Nonlinear Waves and Weak Turbulence with Applications in Oceanography and Condensed Matter Physics* (ed. N. Fitzmaurice, D. Gurarie, F. McCaughan & W. Woyczynski), pp. 159–177 Birkhauser.

Graebel, W. P. 1966 On determination of the characteristic equations for the stability of parallel flows. *J. Fluid Mech.* **24**, 497–508.

HABERMAN, R. 1972 Critical layers in parallel flows. *Stud. Appl. Maths* **51**, 139–161.

KACHANOV, YU. S., KOZLOV, V. V. & LEVCHENKO, V. YA. 1977 Nonlinear development of a wave in a boundary layer. *Izv. AN SSSR, Mekh. Zhidk i Gaza* **3**, 49–53.

KACHANOV, YU. S. & LEVCHENKO, V. YA. 1984 The resonant interaction of disturbances at laminar-turbulent transition in a boundary layer. *J. Fluid Mech.* **138**, 209–247.

KHOKHLOV, A. P. 1993 Evolution of resonant triads in a boundary layer. Submitted to *J. Fluid Mech.*

KOPAL, Z. 1961 *Numerical Analysis,* 2nd edn. Chapman & Hall.

LEIB, S. J. & LEE, S. S. 1995 Nonlinear evolution of a pair of oblique instability waves in a supersonic boundary layer. *J. Fluid Mech.* **282**, 339–371.

LIN, C. C. 1955 *The Theory of Hydrodynamic Stability*. Cambridge University Press.

MANKBADI, R. R., WU, X. & LEE, S. S. 1993 A critical-layer analysis of the resonant triad in boundary-layer transition: nonlinear interactions. *J. Fluid Mech.* **256**, 85–106.

MILES, J. W. 1962 A note on the inviscid Orr-Sommerfeld equation. *J. Fluid Mech.* **13**, 427–432.

NIELD, D. A. 1972 On the inviscid solutions of the Orr-Sommerfeld equation. *Math. Chronicle* **2**, 43–52.

RAETZ, G. S. 1959 A new theory of the cause of transition in fluid flows. *Northrop Corp.* NOR-59-383 BLC-121.

REID, W. H. 1965 The stability of parallel flows. In *Basic Developments in Fluid Dynamics* (ed. M. Holt), Vol. 1, pp. 249–307. Academic.

WU, X. 1992 The nonlinear evolution of high-frequency resonant-triad waves in an oscillatory Stokes layer at high Reynolds number. *J. Fluid Mech.* **245**, 553–597.

WU, X. 1993 On critical-layer and diffusion-layer nonlinearity in the three-dimensional stage of boundary-layer transition. *Proc. R. Soc. Lond.* A **443**, 95–106.

WU, X. 1995 Viscous effects on fully coupled resonant-triad interactions: an analytical approach. *J. Fluid Mech.* **292**, 377–407.

WU, X., LEE, S. S. & COWLEY, S. J. 1993 On the weakly nonlinear three-dimensional instability of shear layers to pairs of oblique waves: the Stokes layer as a paradigm. *J. Fluid Mech.* **253**, 681–721.

WU, X., LEIB, S. J. & GOLDSTEIN, M. E. 1997 On the nonlinear evolution of a pair of oblique Tollmien-Schlichting waves in boundary layers. *J. Fluid Mech.* **340**, 361–394.

WUNDROW, D. W., HULTGREN, L. S. & GOLDSTEIN, M. E. 1994 Interaction of oblique instability waves with a nonlinear plane wave. *J. Fluid Mech.* **264**, 343–372.